Since January 2020 Elsevier has created a COVID-19 resource centre with free information in English and Mandarin on the novel coronavirus COVID-19. The COVID-19 resource centre is hosted on Elsevier Connect, the company's public news and information website.

Bioorganic Chemistry 114 (2021) 105131

Contents lists available at ScienceDirect

Bioorganic Chemistry

journal homepage: www.elsevier.com/locate/bioorg

3-Alkenyl-2-oxindoles: Synthesis, antiproliferative and antiviral properties against SARS-CoV-2

Adel S. Girgis [a,*], Siva S. Panda [b], Aladdin M. Srour [c], Anwar Abdelnaser [d], Soad Nasr [d,e], Yassmin Moatasim [f], Omnia Kutkat [f], Ahmed El Taweel [f], Ahmed Kandeil [f], Ahmed Mostafa [f], Mohamed A. Ali [f], Nehmedo G. Fawzy [a], Mohamed S. Bekheit [a], ElSayed M. Shalaby [g], Lara Gigli [h], Walid Fayad [i], Ahmed A.F. Soliman [i]

[a] Department of Pesticide Chemistry, National Research Centre, Dokki, Giza 12622, Egypt
[b] Department of Chemistry & Physics, Augusta University, Augusta, GA 30912, USA
[c] Department of Therapeutic Chemistry, National Research Centre, Dokki, Giza 12622, Egypt
[d] Institute of Global Health and Human Ecology, School of Sciences and Engineering, The American University in Cairo (AUC), Cairo 11835, Egypt
[e] Institute of Pharmacology of Natural Products & Clinical Pharmacology, Ulm University, D-89081 Ulm, Germany
[f] Center of Scientific Excellence for Influenza Viruses, National Research Centre, Giza 12622, Egypt
[g] X-Ray Crystallography Lab., Physics Division, National Research Centre, Dokki, Giza 12622, Egypt
[h] Elettra-Sincrotrone Trieste, s.s. 14 Km 163.5 in Area Science Park, Basovizza (Trieste) 34149, Trieste, Italy
[i] Drug Bioassay-Cell Culture Laboratory, Pharmacognosy Department, National Research Centre, Dokki, Giza, 12622. Egypt

ARTICLE INFO

Keywords:
Indole
Benzimidazole
Antitumor
SARS-CoV-2
VEGFR-2
c-Kit
Docking

ABSTRACT

Sets of 3-alkenyl-2-oxindoles (**6**,**10**,**13**) were synthesized in a facile synthetic pathway through acid dehydration (EtOH/HCl) of the corresponding 3-hydroxy-2-oxoindolines (**5**,**9**,**12**). Single crystal (**10a**,**c**) and powder (**12a**,**26f**) X-ray studies supported the structures. Compounds **6c** and **10b** are the most effective agents synthesized (about 3.4, 3.3 folds, respectively) against PaCa2 (pancreatic) cancer cell line relative to the standard reference used (Sunitinib). Additionally, compound **10b** reveals antiproliferative properties against MCF7 (breast) cancer cell with IC_{50} close to that of Sunitinib. CAM testing reveals that compounds **6** and **10** demonstrated qualitative and quantitative decreases in blood vessel count and diameter with efficacy comparable to that of Sunitinib, supporting their anti-angiogenic properties. Kinase inhibitory properties support their multi-targeted inhibitory activities against VEGFR-2 and c-kit in similar behavior to that of Sunitinib. Cell cycle analysis studies utilizing MCF7 exhibit that compound **6b** arrests the cell cycle at G1/S phase while, **10b** reveals accumulation of the tested cell at S phase. Compounds **6a** and **10b** reveal potent antiviral properties against SARS-CoV-2 with high selectivity index relative to the standards (hydroxychloroquine, chloroquine). Safe profile of the potent synthesized agents, against normal cells (VERO-E6, RPE1), support the possible development of better hits based on the attained observations.

1. Introduction

Many 3-alkenyl-2-oxindole analogs were naturally isolated revealing diverse biological properties [1]. Sunitinib (Sutent) which is a 3-alkenyl-2-oxindole derivative is an orally multi-target tyrosine kinase inhibitor approved by FDA (Food and Drug Administration on Jan. 26, 2006 and Nov. 16, 2017) for the treatment of gastrointestinal and advanced renal cancers. It has been also approved for the treatment of pancreatic cancer (May 20, 2011) [2,3]. Semaxanib, another member of this family, is a VEGFR (vascular endothelial growth factor receptor) inhibitor discontinued in 2002 during phase III clinical trials for colorectal cancer [4] (Fig. 1). Cancer is one of the most serious human health challenges universally. It is the second life deadly disease after cardiovascular disorders. WHO (World Health Organization) reported 1/6 deaths globally is due to cancer in 2018 (9.6 million deaths) [5,6]. Although many targeted drugs are developed and clinically approved, the associated side effects and limited efficacies diminished their applications and demanded the need for novel chemical entities with safer cures and

* Corresponding author.
E-mail address: girgisas10@yahoo.com (A.S. Girgis).

https://doi.org/10.1016/j.bioorg.2021.105131
Received 17 May 2021; Accepted 24 June 2021
Available online 30 June 2021

higher potencies [7].

Many of the investigated anticancer agents/drugs obey "one-molecule – one target – one disease" phenomenon. This allows the emerging of an agent selectively targeting a single biological entity to avoid the risk of off-target side effects. However, this hypothesis seems inadequate for multi-genic diseases (such as cancer, Alzheimer's or Parkinson's disease). This is why multi-targeted inhibitors were developed which can exhibit therapeutic potencies towards various mechanisms [8,9]. It has been reported that cancer initiation and progression depend on several receptors or singling pathways. This is why multi-targeted agents can provide several advantages over mono-targeted therapies. Several multi-target inhibitors (e.g. Sunitinib, Sorafenib, Altiratinib, Linifanib,

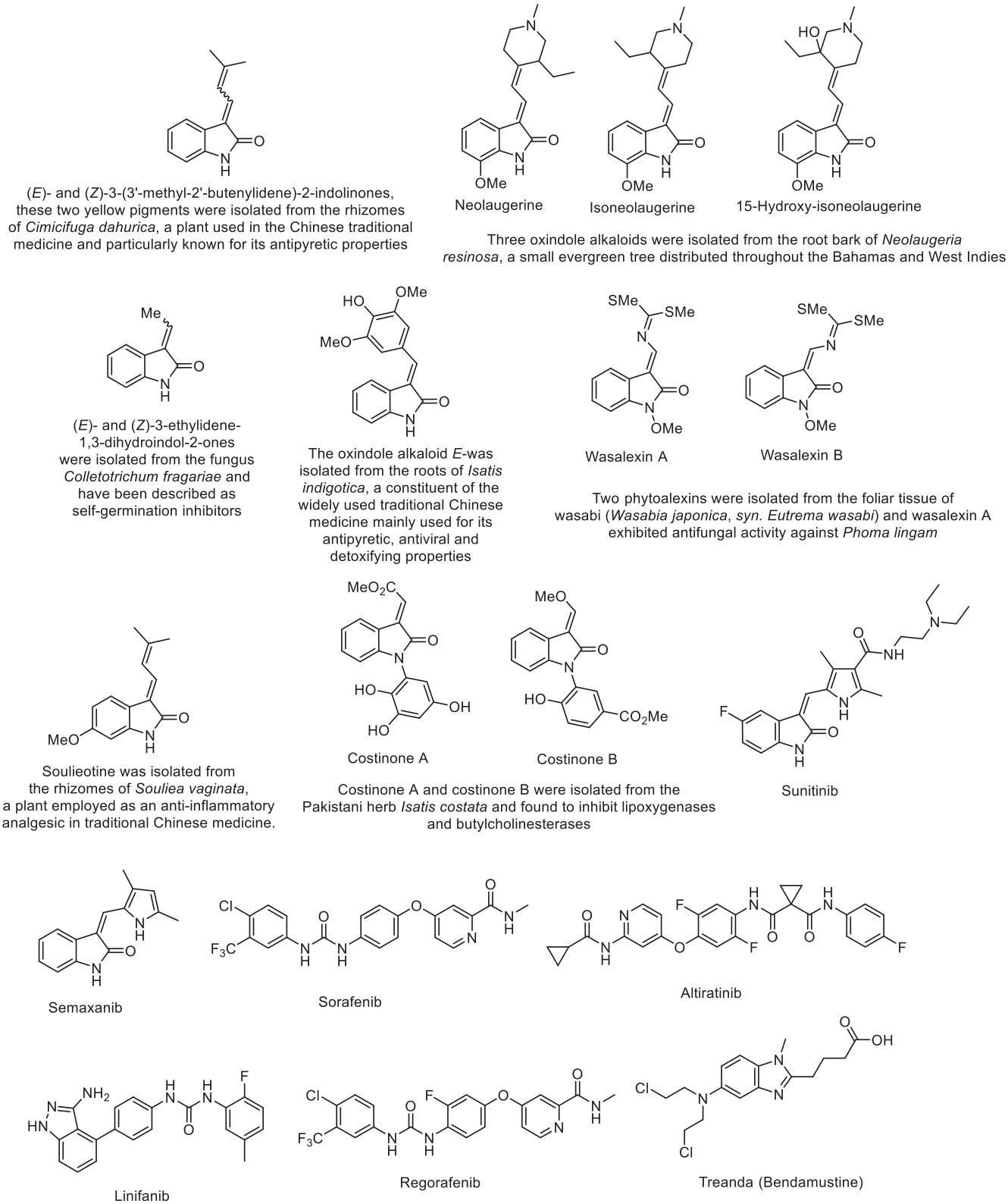

Fig. 1. Biologically active 3-alkenyl-2-oxindoles, multi-targeted anticancer agents and Treanda (Bendamustine).

and Regorafenib) were developed/approved, or investigated in clinical trials [10] (Fig. 1).

In our pursuit to develop novel antitumor agents [11–13], the present study describes the synthesis of 3-alkenyl-2-oxindoles conjugated with sulfonamide function. This fragment is an important component in many clinically approved antitumor drugs {e.g. Belinostat (Beleodaq) [14,15], Dabrafenib (Tafinlar) [16,17], Pazopanib (Votrient) [18,19], Vemurafenib (Zelboraf) [20,21] and Venetoclax (Venclexta) [22,23]}.

Benzimidazolyl heterocycle is also considered for conjugation with the targeted compounds due to the diverse biological properties exhibited by its derivatives such as antitumor [24–31], anti-inflammatory [32], antitubercular [33–35], anti-HIV (human immunodeficiency virus) [36–38], α-glucosidase inhibition [39–41], cholinesterase inhibitor useful to combat the neuromuscular disorders [42], pancreatic lipase inhibitor useful for fat absorption control [43], α-amylase inhibitor useful for diabetes, obesity, and oral diseases [44] and Rho-kinase inhibitor useful for treatment of glaucoma [45]. Treanda (Bendamustine hydrochloride) is a benzimidazolyl derivative approved by FDA (2008) for chronic lymphocytic leukemia [46,47].

Antiproliferative properties of the targeted agents are considered against pancreatic (PaCa), colon (HCT116), and breast (MCF7) carcinoma cell lines. Adoption of the mentioned cell lines for testing is due to the high correlation of the synthesized agents with Sunitinib that show efficacy/clinical application against them. Additionally, pancreatic cancer is the twelfth most common cancer globally with 460,000 new cases in 2018 [48]. It usually develops from exocrine (more common) or neuroendocrine (less common with better prognosis) cells [49]. Colorectal cancer is a malignant tumor arising from genetic and epigenetic changes in colorectal epithelial cells [50]. Heredity, colon polyps, and long-standing ulcerative colitis are major factors that cause colon cancer [51]. Breast cancer is the second cause of female cancer (2.09 million cases) with death incidence 627,000 globally in 2018 according to WHO statistics [5].

The chick chorioallantoic membrane (CAM) assay model can be employed as an *in vivo* xenograft model for cancer cells. The cells form tumor xenografts by seeding onto the chorioallantoic membrane as a result, invasion occurs into a highly vascularized membrane. The CAM model can also be used to study angiogenesis due to the high vascularization of its membrane. The chorioallantoic membrane is composed mostly of type IV collagen, which resembles the human epithelium basement membrane [52–57].

The SARS-CoV-2 (severe acute respiratory syndrome coronavirus-2) seems the most major health care disaster declared by WHO (World Health Organization) as a pandemic COVID-19 [58]. The story began in December 2019 (Wuhan, China) due to novel pneumonia by an unknown pathogen [59]. COVID-19 is a viral disease that belongs to the family *Coronaviridae* and genus *Betacoronavirus* [60]. By May 2021 about 162.2 million patients with 3.364 million deaths were reported worldwide [61]. Lack of available antiviral drugs/vaccines enforced the pharmaceutical authorities/companies to test any agent/drug with antiviral background (drug repurposing). Few agents were considered due to urgent needs (Fig. 2) to control global pandemic but most of them are with low potency and adverse effects [62]. This seems the top today's priority for the political and health authorities to save thousand (s)/million(s) of human life and economic collapse. Recently, few *N*-substituted isatins were reported as SARS-CoV-2 3CLpro inhibitors [63]. Due to this, the 3-alkenyl-2-oxindoles synthesized in the present study are screened for their antiviral properties against SARS-CoV-2. The recent reports describing the possibility for treating SARS-CoV-2 patients with anticancer drugs [64,65] in addition to the successful clinical trial for treating colorectal

carcinoma patients with antiviral drugs solely or in combination with anticancer drugs [66], also prompted the current study targeting developing novel hits of dual functions (antiviral and antitumor) with much attention to their safety profile towards normal cells.

2. Results and discussion

2.1. Chemistry

Reaction of 4-acetylphenyl alkanesulfonates **3a,b** with isatins **4a,b** in absolute ethanol containing quantitative amount of diethylamine at room temperature afforded the corresponding 4-[2-(3-hydroxy-2-oxoindolin-3-yl)acetyl]phenyl alkanesulfonates **5a-d** in good yields (Scheme 1). Compounds **5a-d** were isolated from the conducted reactions in adequate purity so, used directly in the next step without any further purification. IR spectrum of **5a** (example of the agents prepared) reveals the ketonic and indolyl carbonyl bands at $\nu = 1701, 1675\ cm^{-1}$ beside the hydroxyl, and indolyl NH as a broad–band at $\nu = 3291\ cm^{-1}$. The methylene protons are diastereotopic shown as two doublet signals at $\delta_H = 3.61, 4.09$ ($J = 17.5$ Hz). The ^{13}C NMR spectrum of **5a** exhibits the indolyl *C*-3 and *C*-

2 at $\delta_C = 72.9, 178.2$ respectively beside, the methylene and ketonic carbonyl at $\delta_C = 45.7, 195.4$, respectively.

Acidic dehydration (EtOH/HCl) of **5** afforded directly (*E*)-4-[2-(2-oxoindolin-3-ylidene)acetyl]phenyl alkanesulfonates **6** in excellent yields. ^1H NMR spectrum of **6a** shows the olefinic proton as a sharp singlet at $\delta_H = 7.74$. The indolyl and ketonic carbonyls are shown at $\delta_C = 168.1, 190.0$, respectively.

Similarly, *N*-[4-(2-(3-hydroxy-2-oxoindolin-3-yl)acetyl]phenyl)-*N*-

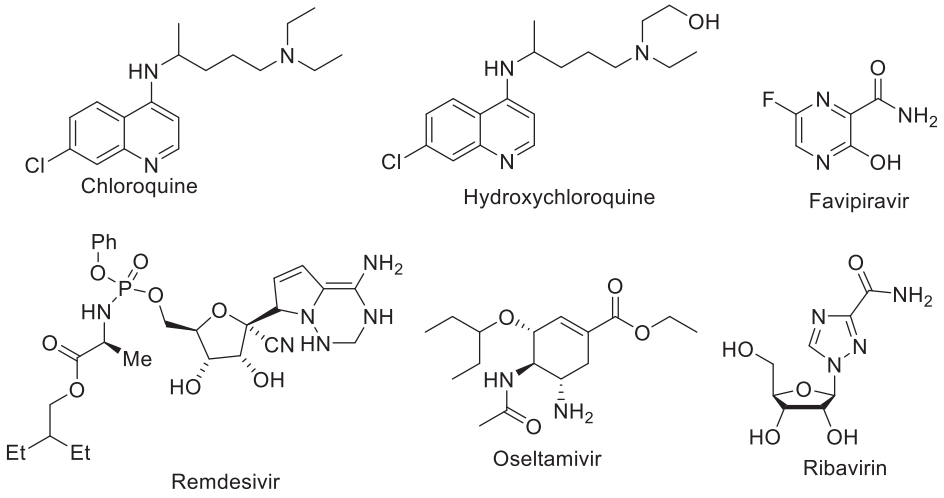

Fig. 2. Repurposing drugs for COVID-19.

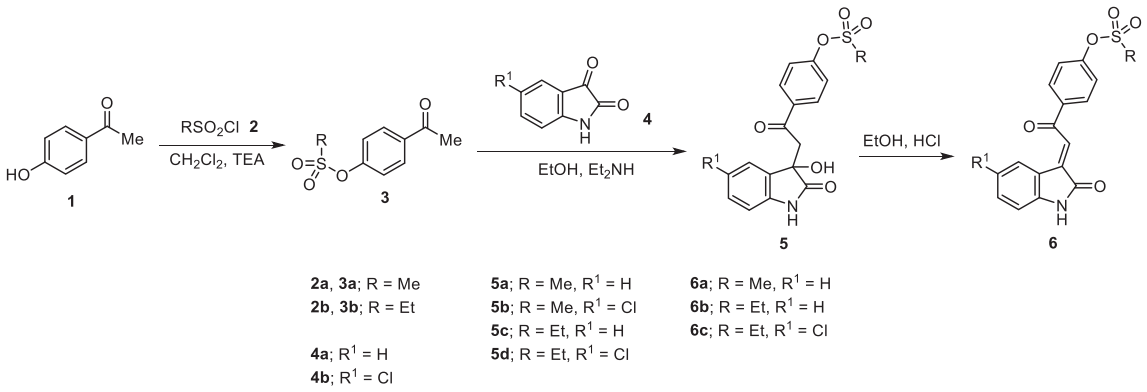

Scheme 1. Synthetic route towards **5** and **6**.

(alkylsulfonyl)alkanesulfonamides **9a-d** were obtained through the reaction of *N*-(4-acetylphenyl)-*N*-(alkylsulfonyl)alkanesulfonamide **8a,b** with the corresponding isatins **4a,b**. Meanwhile, reaction of *N*-(4-acetylphenyl)propane-1-sulfonamide (**8c**) with isatins **4a-c** afforded the corresponding *N*-{4-[2-(3-hydroxy-2-oxoindolin-3-yl)acetyl]phenyl}-*N*-(propylsulfonyl)propane-1-sulfonamide **9e-g**. This is presumably formed due to propylsulfonate elimination from **8c**, under the effect of the reaction basic catalysis used followed by a simultaneous attack to another molecule giving eventually the isolated products **9e-g**. Acidic dehydration of **9** afforded the corresponding **10** in good yields (Scheme 2). ^{1}H NMR of **10a-c** reveal the olefinic proton as a singlet signal at δ_H = 7.74–7.80. Single crystal X-ray studies of compounds **10a,c** support the *E*-configuration (Fig. 3).

3-Hydroxy-3-[2-(1-alkyl-1*H*-benzo[*d*]imidazol-2-yl)-2-oxoethyl] indolin-2-ones **12a-h** were also obtained through base-catalyzed reaction of 1-alkyl-2-acetylbenzimidazoles **11a,b** with isatins **4a-e** which are formed in sufficient purity and used directly in the next step. Powder X-ray studies of compounds **12a,f** add conclusive support for the structure (Fig. 4). 3-[2-(1-Alkyl-1*H*-benzo[*d*]imidazol-2-yl)-2-oxoethylidene] indolin-2-ones **13a–f** could also be synthesized from the corresponding **12a-f** through acidic dehydration. Acidic dehydration of **12 g,h** under the same reaction conditions afforded **13a** as a sole product. This is probably formed *via* cyclic-amino methylene elimination under the effect of the applied acidic reaction conditions (Scheme 3). ^{1}H NMR spectra of **13a-f** reveal the olefinic proton as a sharp singlet at δ_H = 8.66–8.85. The downfield shift shown by these analogs relative to **6a-c** and **10a-c** can be attributed to the anisotropic effect of benzimidazolyl heterocycle (the spectral illustrations are presented in supplementary Figs. S1–S108).

2.2. X-ray studies

Single crystals suitable for Synchrotron single-crystal X-ray diffraction experiments were obtained for the compounds **10a** and **10c**. Compounds **10a** and **10c** crystallized in the monoclinic *P*21/*c* and triclinic *P*-1 space groups, respectively. ORTEP views of the compounds are shown in Fig. 3. In both structures, the 4-[2-(2-oxoindolin-3-ylidene) acetyl]phenyl system seems almost planar, forming a dihedral angle of 82.23° and 80.28° with the sulfonamide group of **10a** and **10c**, respectively. In **10a** the torsion angle defined by C29-C30-C31-C32 is nearly planar (179.19°). Whereas, in the other independent molecule the same angle defined by C9-C10-C11-C16 is 150.23° resulting in a loss of planarity. In both compounds, the intermolecular hydrogen bond between the N(1, 3)H and the carbonyl group of the heterocycle with a bond length of 2.02 Å and 1.972 Å, respectively, stabilize the crystal structures (Supplementary Tables S1–S4, S8; Figs. S109, S110).

On the other hand, the indexing of the investigated X-ray powder diffraction data of compounds **12a** and **12f** resulted in the triclinic *P*-1 and monoclinic $P2_1/n$ space group, respectively with one molecule per asymmetric unit in each (Fig. 4). The torsion angles defined by C14-C13-C12-C9 show different values. It is nearly planar (176.5°) in compound **12a** and out of plane in compound **12f** (72.79°). As a consequence, the benzimidazolyl and indolyl heterocycles form a dihedral angle of 79.63° and 49.02° in the **12a** and **12f**, respectively. Moreover, this fact leads to a different intramolecular bond between the benzimidazolyl and indolyl heterocycles as in compound **12a** is ruled by the N7-O15 bond distance

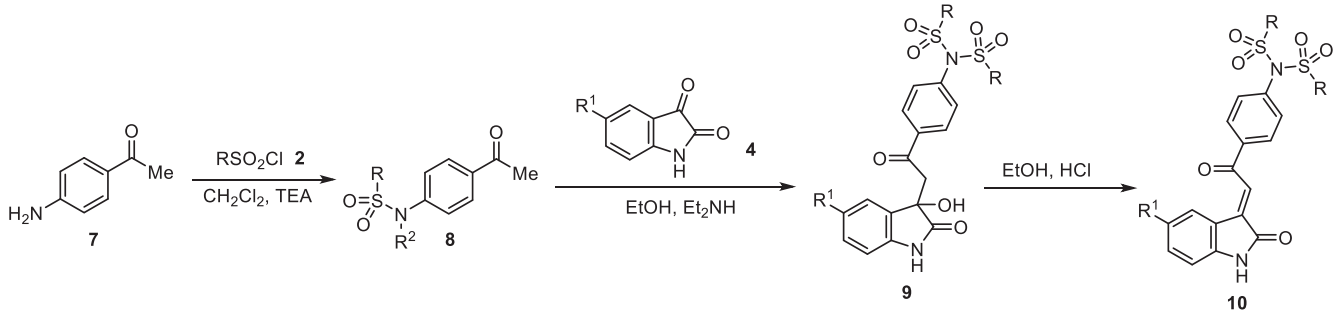

Scheme 2. Synthetic route towards **9** and **10**.

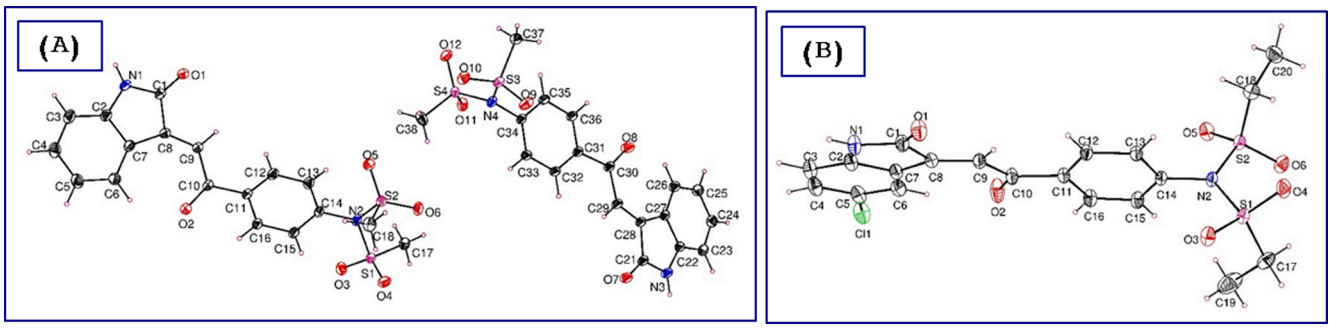

Fig. 3. ORTEP view of compounds (A) **10a** and (B) **10c** showing the atom-numbering scheme. H atoms are shown as small spheres of arbitrary radii.

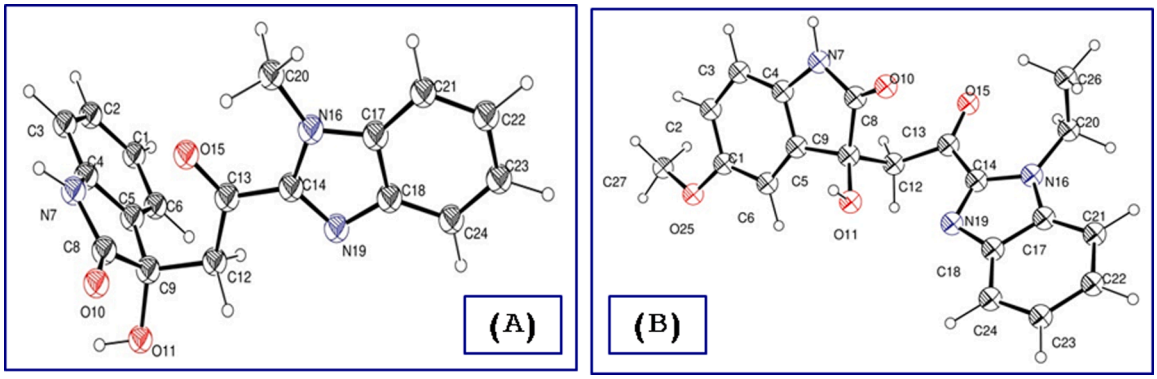

Fig. 4. ORTEP view of compounds (A) **12a** and (B) **12f** showing the atom-numbering scheme. H atoms are shown as small spheres of arbitrary radii.

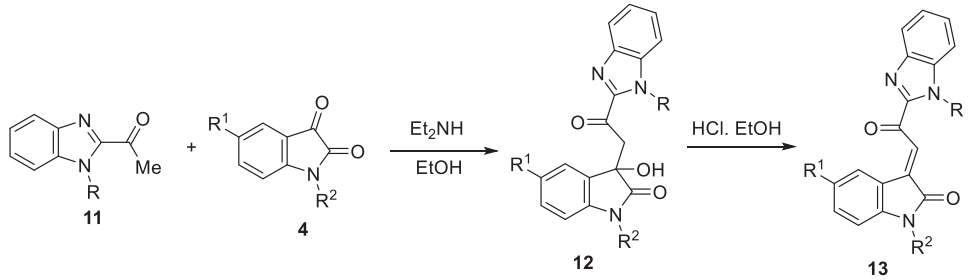

11a; R = Me
11b; R = Et

4a; $R^1 = R^2 = H$
4b; R^1 = Cl, $R^2 = H$
4c; R^1 = OMe, $R^2 = H$
4d; $R^1 = H$, R^2 = (1-piperidinyl)methylene
4e; $R^1 = H$, R^2 = (4-morpholinyl)methylene

12a; R = Me, $R^1 = R^2 = H$
12b; R = Et, $R^1 = R^2 = H$
12c; R = Me, R^1 = Cl, $R^2 = H$
12d; R = Et, R^1 = Cl, $R^2 = H$
12e; R = Me, R^1 = OMe, $R^2 = H$
12f; R = Et, R^1 = OMe, $R^2 = H$
12g; R = Me, $R^1 = H$, R^2 = (1-piperidinyl)methylene
12h; R = Me, $R^1 = H$, R^2 = (4-morpholinyl)methylene

13a; R = Me, $R^1 = R^2 = H$
13b; R = Et, $R^1 = R^2 = H$
13c; R = Me, R^1 = Cl, $R^2 = H$
13d; R = Et, R^1 = Cl, $R^2 = H$
13e; R = Me, R^1 = OMe, $R^2 = H$
13f; R = Et, R^1 = OMe, $R^2 = H$

Scheme 3. Synthetic route towards **12** and **13**.

of 2.69 Å. That is lost in the **12f** and replaced by a slightly shorter N11-O1 bond distance of 2.52 Å. In the **12f** there is a strong intermolecular H-bond between the N(7)–H and the carbonyl group of the heterocycle with a bond length of 1.786 Å (Supplementary Tables S5–S7, S9; Figs. S111, S112).

2.3. Biological studies

2.3.1. Antiproliferative properties

Standard MTT technique was considered for determining the antiproliferative properties of the synthesized compounds utilizing Sunitinib as a standard reference against pancreatic (PaCa-2), breast (MCF7), and colon (HCT116) cancer cell lines [67]. Table 1 reveals the cytotoxic

Table 1
Antiproliferative properties of the tested compounds.

Entry	Compd.	IC_{50} (μM) ± SE		
		PaCa-2	MCF7	HCT116
1	**6a**	8.30 ± 0.44	6.85 ± 0.37	16.38 ± 0.70
2	**6b**	5.60 ± 0.57	4.25 ± 0.23	12.77 ± 1.41
3	**6c**	4.99 ± 0.29	4.28 ± 0.51	5.33 ± 0.46
4	**10a**	6.91 ± 0.89	6.07 ± 0.83	20.96 ± 1.75
5	**10b**	5.08 ± 0.57	4.15 ± 0.78	13.83 ± 1.06
6	**10c**	6.18 ± 0.32	4.43 ± 0.47	>50.00 ± 0.84
7	**Sunitinib**	16.91 ± 0.95	3.97 ± 0.14	5.03 ± 0.30

properties of the targeted 3-alkenyl-2-oxindoles in IC_{50} (μM, concentrations exhibiting 50% cell growth inhibition relative to the control experiment). It has been noticed that all the synthesized 3-alkenyl-2-oxindoles **6a–c** and **10a–c** show remarkable antiproliferative properties against pancreatic cancer (PaCa-2) cell line with potency higher than that of Sunitinib. Compounds **6c** and **10b** are the most effective agents synthesized (about 3.4, 3.3 folds, respectively) relative to Sunitinib. Compound **6b** also reveals high potency against PaCa2, three time folds relative to Sunitinib. On the other hand compound **10b** is the most potent agent synthesized against MCF7 (breast) cancer cell line exhibiting IC_{50} close to that of the standard reference used (IC_{50} = 4.15, 3.97 μM for **10b** and Sunitinib, respectively). Compounds **6b** and **6c** also reveal similar behavior with efficacy close to that of Sunitinib (IC_{50} = 4.25, 4.28 μM for **6b** and **6c**, respectively). However, compound **6c** is the only synthesized analog with cytotoxic properties against HCT116 (colon) cancer cell line close to the standard reference used (IC_{50} = 5.33 and 5.03 μM corresponding to **6c** and Sunitinib, respectively).

Based on the biological observations few SAR (structure–activity relationships) can be assigned. Attachment of the ethyl group to the sulfonate/sulfonamide fragment is critical in developing biological properties comparable with the methyl group as revealed in pairs **6a**/**6b** and **10a**/**10b**. It has also been noticed that in case of PaCa2 (pancreatic) and HCT116 (colon) cancer cell lines, attachment of chlorine atom to the indolyl heterocycle enhances the observed antiproliferative properties of the sulfonate containing-compounds as shown in the pair **6b**/**6c**. On the other hand, utilization of benzimidazolyl heterocycle instead of the substituted phenyl quenched the targeted biological properties (as revealed in compounds **6a–c** and **10a–c** relative to compounds **13a–f**). This can be attributed to the high insolubility (with high melting point) of the synthesized compounds **13** in aqueous media.

The cytotoxic properties of the effective agents synthesized (**6a–c** and **10a–c**) were also determined against non-cancer RPE1 (retinal pigment epithelium) cell line. The observed data support the safety profile of all the tested analogs against the utilized normal cell line (IC_{50} > 50 μM). Antiproliferative properties of all the tested agents are shown in Supplementary Figs. S113–S116.

2.3.2. CAM assay

CAMs treated with the proposed synthesized agents (the most promising antiproliferative agents synthesized) **6a–c** and **10a–c**, control (vehicles, DMSO, PBS "Phosphate-buffered saline", and ethanol) and positive control (Sunitinib) showed a significant difference in blood vessel number and diameter, either quantitatively (n = 4) or qualitatively (Fig. 5A). In detail, CAMs treated with vehicle only showed the highest blood vessel diameters (14 mm). CAMs treated with Sunitinib showed reduction in blood vessel diameters in comparison to control (5 mm). Compounds **6a–c** significantly reduced the blood vessel diameters to 3.2, 5.1, and 5.13 mm, respectively, compared to control. Compounds **10a–c** also reduced the blood vessel diameters to 3.5, 2.7, and 5 mm, respectively, compared to control (Fig. 5B, Table 2). In order to support these observations, H&E (haematoxylin and eosin) staining for CAMs was performed. In this regard, H&E staining confirmed the mentioned observations (revealing reductions in the number of blood vessels) for the CAMs treated with the positive control (Sunitinib) and the tested agents **6a–c**, **10a–c**.

The CAM assay is one of the most utilized techniques for determination of anti-angiogenic effects [68]. This is attributed to the highly vascularized membrane and that the chorioallantoic membrane is mostly composed of type IV collagen, which resembles the human epithelium basement membrane [52–57]. Our results show that the promising antiproliferative synthesized agents **6a–c** and **10a–c** possess anti-angiogenic properties as they can decrease the number and diameter of the blood vessels with potency comparable to that of Sunitinib, which is a well-known drug with anti-angiogenic properties [69–71]. In conclusion, the synthesized agents **6** and **10** can be considered as potential anti-tumor agents with anti-angiogenic properties.

2.3.3. Kinase inhibitory properties

Angiogenesis is the formation of novel blood vessels/branches from the existing ones [72]. The new blood vessels are useful for nutrient and oxygen transportation to the endothelial cells that may stimulate and proliferate forming new sprouts. Regulated angiogenesis is an important process for embryonic development, reproduction, and wound healing due to cell growth and tissue re-generation [73]. On the other hand, dysregulated angiogenesis is observed in many diseases including solid cancers. This is why targeting dysregulated angiogenesis seems an important therapeutical approach for competing diverse cancer types and sometimes has been considered preferable to other chemotherapies to avoid the adverse effects on normal/healthy cells [74]. It has been reported that vascular endothelial growth factor receptors are three main categories (VEGFR-1, VEGFR-2, and VEGFR-3) responsible for tumor angiogenesis [75,76]. VEGFR-2 is the main receptor capable for anti-angiogenesis and controlling tumor proliferation [74].

Table 3 (Fig. 6) exhibits the VEFGR-2 inhibitory properties of the promising antiproliferative 3-alkenyl-2-oxindoles (**6a–c**, **10a–c**) synthesized. From the exhibited data it has been noticed that, compound **6c** is the most potent VEGFR-2 inhibitor with 1.3 folds relative to that of Sunitinib (standard reference used). This observation is comparable to that shown by CAM testing (blood vessel diameter = 5.1, 5.0 mm by compound **6c** and Sunitinib, respectively). Compound **10c** also reveals promising VEGFR-2 inhibitory properties (IC_{50} = 53.36 *n*M, i.e. 0.89 fold relative to Sunitinib). This observation is comparable to the antiproliferative properties revealed for MCF7 (breast) cancer cell line (IC_{50} = 4.43, 3.97 μM for compound **10c** and Sunitinib, respectively; i.e. 0.9 fold potency) and CAM testing (blood vessel diameter = 5.0 mm by both compound **10c** and Sunitinib). Additionally, the promising VEGFR-2 exhibited by compound **6a** (IC_{50} = 54.03 *n*M) also supports the revealed antiproliferative properties against MCF7 (IC_{50} = 6.85 μM).

The c-Kit receptor is a member of class III tyrosine kinase receptor [77]. Overexpression of c-kit initiates cell proliferation and tumor creation [78]. Suppressing the c-kit was reported as an efficient therapeutic strategy for controlling many cancer types [79–81]. It has been reported that, the VEGFR-2 inhibitors may block/inhibit other tyrosine kinase receptors (e.g. c-Kit, PDGFRs, FGFRs, and Flt-3); due to the structural similarities so, can be recognized as multi-targeted tyrosine kinase inhibitors with accessibility against different cancer types [82]. Additionally, the chemical structural resemblance of the antiproliferative agents synthesized and Sunitinib also prompted screening the inhibitory properties of **6a–c** and **10a–c** towards c-kit. Considering that Sunitinib is approved as multi-targeted inhibitor against various kinases including VEGFR, PDGFR, FLT-3 and c-kit [83].

Table 3 (Fig. 6) reveals the inhibitory properties of the tested compounds against c-kit. It has been noticed that, compound **6c** is a potent c-kit inhibitor with efficacy higher than that of the standard reference used, Sunitinib (IC_{50} = 72.35, 84.9 *n*M for **6c** and Sunitinib, respectively). These observations can support the exhibited antiproliferative properties of **6c** relative to Sunitinib as mentioned in the VEGFR-2 inhibitory observations. Compound **10c** also reveals promising c-kit inhibitory properties close to that of Sunitinib (IC_{50} = 81.7, 84.9 *n*M for **10c** and Sunitinib, respectively). These observations are comparable to their antiproliferative properties against MCF7 (breast) cancer cell line (IC_{50} = 4.43, 3.97 μM for compound **10c** and Sunitinib, respectively). Generally, most of the revealed kinase (VEGFR-2 and c-kit) inhibitory properties observed by the tested compounds are consistent with their antitumor observations (Table 1). The slight differences shown are due to the environmental experimental conditions applied (standard protocols). It can also conclude that the synthesized agents are multi-targeted kinase receptor inhibitors (VEGFR-2 and c-kit).

2.3.4. Cell cycle study

Cell cycle analysis *via* quantitative DNA content is an important technique capable to identify the proliferation of culture cells and cell distribution in each phase of the cell cycle. Propidium iodide (PI)

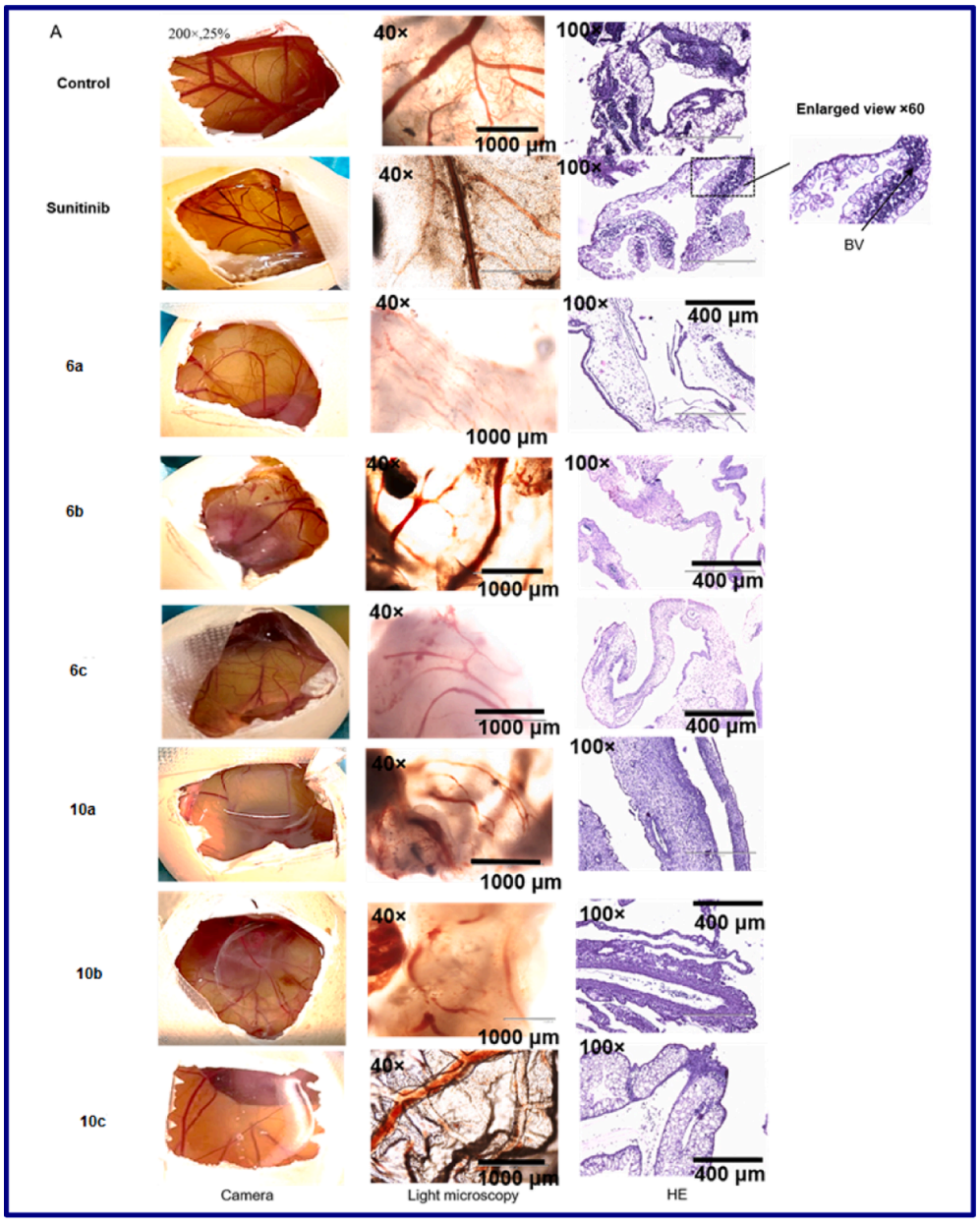

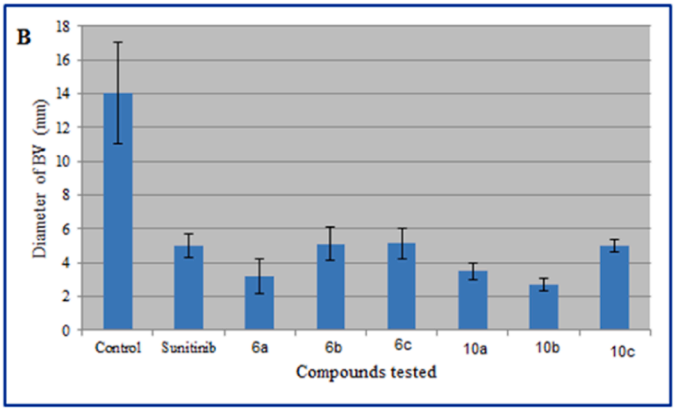

Fig. 5. (A) Images and histology using H&E of the chick embryo chorioallantoic membrane (CAM) for vehicle control, positive control (Sunitinib) and test compounds. At day 8, eggs were opened carefully. Twenty µl of control vehicle or test compounds (final concentration of 660 µM) were left to dry on a 2.5 cm round glass slide on the surface of the CAM blood network. Eggs were covered and left in an incubator at 37 °C for 3 days. Later the membrane around the area of interest was fixed with 5% formalin, and paraffin embedded for further staining. Original images were done at 40x and 100x magnification "CM: chorionic membrane. ML: mesodermal layer. BV: blood vessel". (B) Quantitative analysis of blood vessel diameter in mm after 3 days of treatment. Sunitinib (positive control) and test compounds all show significant reduction in BV diameters. All results are expressed as mean ± SD (n = 4) (***$P < 0.001$ in comparison to control).

Table 2
Blood vessel diameter of tested compound and Sunitinib.

Entry	Compd.	Mean diameter of blood vessels (mm ± SD "standard division")
1	**Control**	14.00 ± 3.00
2	**Sunitinib**	5.00 ± 0.71
3	**6a**	3.20 ± 1.00
4	**6b**	5.10 ± 1.00
5	**6c**	5.13 ± 0.90
6	**10a**	3.50 ± 0.50
7	**10b**	2.70 ± 0.40
8	**10c**	5.00 ± 0.40

Table 3
Kinase inhibitory properties of the promising antiproliferative 3-alkenyl-2-oxindoles (**6a–c**, **10a–c**) synthesized and Sunitinib.

Entry	Compd.	IC_{50} (*n*M ± SD)	
		VEGFR-2	c-kit
1	**6a**	54.03 ± 5.4	119.8 ± 12.0
2	**6b**	98.95 ± 9.9	247.7 ± 24.8
3	**6c**	36.86 ± 3.7	72.35 ± 7.2
4	**10a**	102.2 ± 10.2	103.3 ± 10.3
5	**10b**	74.06 ± 7.4	184.9 ± 18.5
6	**10c**	53.36 ± 5.3	81.7 ± 8.2
7	**Sunitinib**	47.54 ± 4.8	84.9 ± 8.5

staining of DNA utilizing flow cytometry cell cycle analysis is an accessible technique for stoichiometric DNA cell content determination [84]. Arresting cell cycle during the transition from G1 phase to S phase seems an important mode for many antiproliferative active agents [85]. Compounds **6b** and **10b** (the most effective antiproliferation agents synthesized against breast cancer cell line) were subjected for induced cell cycle study of MCF7 utilizing the assigned IC_{50} value (Table 1). This identifies the cell cycle distribution and phase arresting during the antiproliferation inhibitory process of the bio-active agents. From the results obtained (Table 4, Figs. 7, 8) it has been noticed that, compound **6b** reveals decrease in the accumulated tested cells at G2/M relative to the control experiment (% G2/M = 2.67, 5.09 for compound **6b** and control experiment, respectively; i.e. 47.5% decrease in cell population). However, slight accumulation of the tested cell at G1/S phase was observed relative to the control (%G0-G1 = 54.08, 53.79; %S = 43.25, 41.12 for compound **6b** and control experiment, respectively). This identifies that compound **6b** arrests the cell cycle at G1/S phase. On the other hand, compound **10b** reveals accumulation of the tested cell at S phase higher than that of G0/G1 phase "also with about 13% increment in S phase

than that of the control experiment" (%S = 54.18, 41.12 for compound **10b** and control experiment, respectively). This supports the efficacy of compound **10b** to arrest the tested cell at S phase.

Apoptosis induction [86] was also noticed by the bio-active agents synthesized **6b** and **10b** against MCF7 cell utilizing IC_{50} values discovered (Table 1). From the results obtained (Table 5, Fig. 8) it has been noticed that compound **6b** is a higher apoptosis performing agent than **10b**. This is due to the increased late stage of apoptosis observed by **6b** than **10b** (% late stage = 22.91, 17.15 by compounds **6b** and **10b**, respectively). Compound **6b** also reveals higher necrosis induction than **10b** (% necrosis = 9.29, 7.07 by compounds **6b** and **10b**, respectively).

2.3.5. *Antiviral properties*

Antiviral properties of the synthesized 3-alkenyl-2-oxindoles (**6a–c**, **10a–c**) against SARS-CoV-2 were determined by the standard technique [87–89] and compared with that of hydroxychloroquine, chloroquine and Favipiravir, which are used as standard references. Table 6 (Fig. 9) reveals the IC_{50} (concentration needed for 50% reduction of virus-induced cytopathic effect compared to control experiment) and the CC_{50} (concentration needed for 50% growth normal cell line "VERO-E6, needed for viral growth" inhibition relative to control experiment) for all the tested compounds. The SI (therapeutical/selectivity index, which is the ratio of CC_{50} relative to IC_{50}) is an important parameter identifying the selectivity of the tested agent for the viral cell relative to the host normal cell. This is an important indicator explaining the safety profile of a tested agent.

From the observed results, it can be concluded that many of the synthesized agents reveal antiviral properties with potency high than that of hydroxychloroquine (which reveals higher potency relative to the other standard references used, chloroquine and Favipiravir). Compounds **10b** and **6a** are superior among all the tested agents (IC_{50} = 3.417, 3.799 μM, for **10b** and **6a**, respectively). However, compound **6a** seems a preferable agent than **10b** for any higher biological testing due to the higher SI revealed (SI = 362.5, 165.6 for **6a** and **10b**,

Table 4
Percentage cell distribution during induced cell cycle study for compounds **6b** and **10b** on MCF7 cells by PI-flow cytometry.

Entry	Compd.	DNA content (%)			
		G0-G1	S	G2/M	Pre-G1
1	**6a**	54.08	43.25	2.67	34.71
2	**10a**	41.71	54.18	4.11	28.25
3	**Control**	53.79	41.12	5.09	1.49

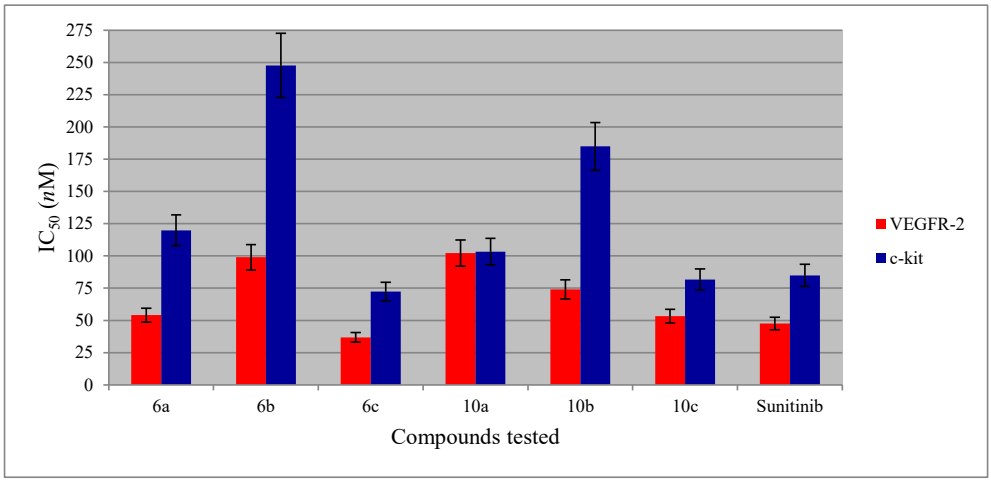

Fig. 6. Kinase inhibitory properties of the tested compounds and Sunitinib.

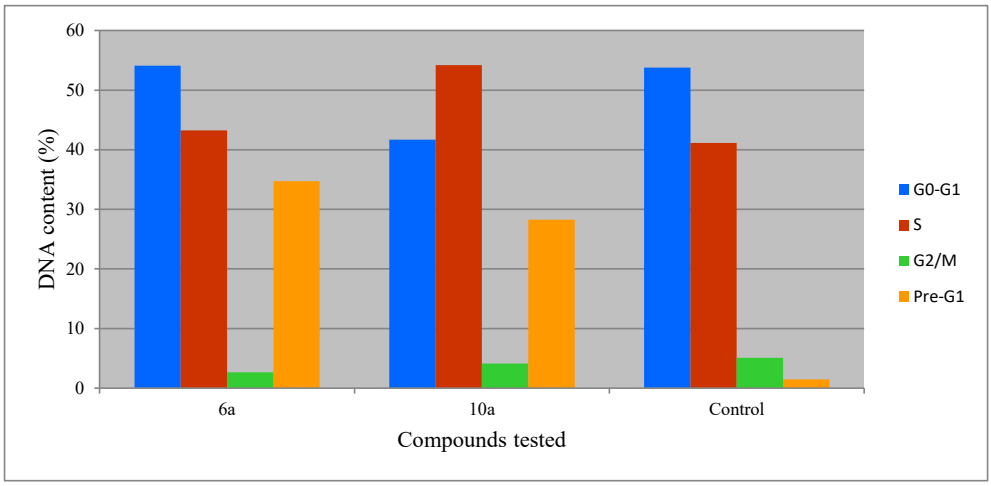

Fig. 7. DNA content during induced cell cycle analysis study (MCF7) for the tested compounds and control experiment by PI-flow cytometry.

respectively). Compound **6c** is also a promising agent with enhanced potency and selectivity index than the standard references used (IC_{50} = 13.52, 29.25, 19.78; SI = 26.4, 12.2, 19.1 for **6c**, hydroxychloroquine and chloroquine, respectively). Compound **10c** exhibits promising SI due to its high cytotoxicity value

(CC_{50}) relative to the antiviral potency (IC_{50}) value (IC_{50} = 20.1, CC_{50} = 1517 μM, SI = 75.5).

2.4. Molecular modeling

Molecular modeling is a computational technique intensively utilized in medicinal chemical studies. It is useful for identifying the parameters necessary for bio-properties *via* exploring the interaction taking place between the proposed bio-active agent and amino acids of the protein active site. This may support the assumed mode of action and assigning the agent's functional group(s) necessary for the observed biological properties. Standard CDOCKER technique was considered in the current study (Discovery Studio 2.5 software; force field, CHARMm; partial charge method, MMFF94) utilizing PDB ID: 4AGD, 3G0E for VEGFR-2 and c-kit modeling respectively [90–93]. Table 7 (Supplementary Figs. S117, S118) exhibits the molecular docking results for the promising antiproliferative agents synthesis (**6a–c**, **10a–c**) and Sunitinib (reference standard used) in the PDB ID: 4AGD and 3G0E responsible for VEGFR-2 and c-kit inhibition, respectively.

2.4.1. VEGFR-2

Table 7 (Supplementary Fig. 117) reveals that, all the tested compounds aligned perfectly in the active site of the used protein in a similar manner/behavior to that of Sunitinib with different docking scores. All the tested compounds give hydrogen bonding interaction between the indolyl C═O and CYS919 of the protein active site. Additionally, compounds **6b** and **10a-c** reveal hydrogen bonding interaction of the indolyl NH with the GLU917 of the protein active site, which is also shown by Sunitinib (co-crystallized ligand in the protein active site). π-Interaction is only revealed by compound **6a**. The minor docking score compatibility difference of the docked agents relative to the kinase inhibitory properties observed (Table 3) can be attributed to the effect of environmental conditions applied in the kinase investigation experimental technique, which are not considered in the computational studies.

2.4.2. c-Kit

All the tested compounds (**6a–c**, **10a–c**) show two hydrogen-bonding interactions with CYS673 and GLU671 of the protein active site with alignment similar to that of Sunitinib and varied docking scores. Additionally, all the tested compounds (**10b** is an exception) support their alignment in the protein active site through π-σ interaction taking place between the indolyl heterocycle and VAL603. Again, the sigh compatibility differences observed due to docking scores and c-kit kinase inhibitory properties of the tested analogues can be attributed to the experimental conditions applied for the biochemical testing which are not considered in the computational work Table 7 (Supplementary Fig. S118).

Generally, the docking studies especially, alignment and hydrogen bonding revealed by the docked agents in the protein active sites, support the multi-targeted kinase inhibitory properties of **6a–c** and **10a–c** in a comparable behavior to that known by Sunitinib.

3. Conclusion

In conclusion, 3-alkenyl-2-oxindoles with sulfonate or sulfonamide function seem promising antiproliferative agents. Compounds **6c** and **10b** are the most effective agents synthesized (about 3.4, 3.3 folds, respectively) against PaCa2 (pancreatic) cancer cell line relative to Sunitinib. Additionally, compound **10b** reveals antiproliferative properties against MCF7 (breast) cancer cell line with IC_{50} close to that of the standard. Meanwhile, compound **6c** is the only synthesized analog with cytotoxic properties against HCT116 (colon cancer) cell line close to the standard reference used. CAM testing reveals that compounds **6** and **10** are capable to reduce blood vessel diameter with efficacy comparable to that of Sunitinib supporting their anti-angiogenic properties. Kinase inhibitory properties of the promising antiproliferative 3-alkenyl-2-oxindoles (**6a–c**, **10a–c**) synthesized support their multi-targeted inhibitory activities against VEGFR-2 and c-kit in similar behavior to that of Sunitinib. Molecular docking studies (PDB ID: 4AGD and 3G0E) support these observations. Cell cycle analysis studies utilizing MCF7 (breast) cancer cell, exhibit that compound **6b** arrests the cell cycle at G1/S phase while, **10b** reveals accumulation of the tested cell at S phase. Additionally, compound **6b** is a higher apoptosis performing agent than **10b**. Compounds **6a** and **10b** reveal potent antiviral properties against SARS-CoV-2 with high therapeutical/selectivity index relative to all the standards used (hydroxychloroquine, chloroquine and Favipiravir). The safety profile of the testing agents, especially the high potent ones, against normal cells (VERO-E6 and RPE1) is a good indication for the possibility of utilization as antitumor and/or antiviral agents. Also, the promising results obtained can be adopted for developing higher effective hits.

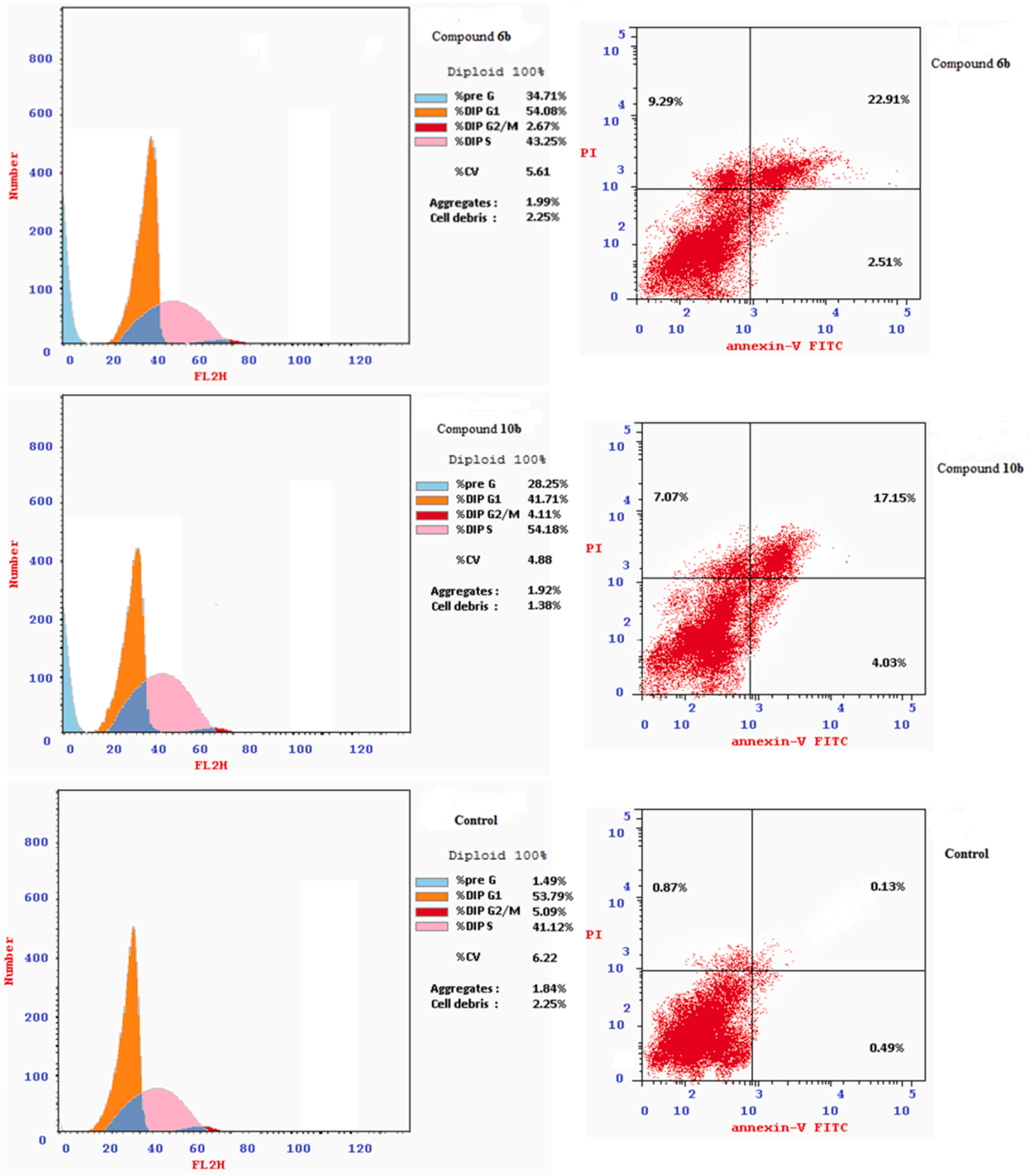

Fig. 8. Cell cycle analysis and apoptosis induced by the tested compounds and control experiment for MCF7.

4. Experimental

4.1. Chemistry

Melting points were determined on a capillary point apparatus (Stuart SMP3) equipped with a digital thermometer. IR spectra (KBr) were recorded on a Shimadzu FT-IR 8400S spectrophotometer. Reactions were monitored using thin layer chromatography (TLC) on 0.2 mm silica gel F254 plates (Merck) utilizing various solvents for elution. The chemical structures of the synthesized compounds were characterized by nuclear magnetic resonance spectra (^{1}H NMR, ^{13}C NMR) and determined on a Bruker NMR spectrometer (500 MHz, 125 MHz for ^{1}H and ^{13}C, respectively). ^{13}C NMR spectra are fully decoupled. Chemical shifts were reported in parts per million (ppm) using the deuterated solvent peak or tetramethylsilane as an internal standard.

Table 5
Percentage apoptosis and necrosis for compounds **6b** and **10b** on MCF7 cells induced by IC_{50} values.

Entry	Compd.	Apoptosis (%)			Necrosis
		Total	Early	Late	
1	**6b**	34.71	2.51	22.91	9.29
2	**10b**	28.25	4.03	17.15	7.07
3	**Control**	1.49	0.49	0.13	0.87

Table 6
Antiviral properties of the tested compounds against SARS-CoV-2.

Entry	Compd.	IC_{50} (μM)[a]	CC_{50} (μM)[b]	SI[c]
1	**6a**	3.799	1377	362.5
2	**6b**	55.14	1313	23.8
3	**6c**	13.52	356.9	26.4
4	**10a**	219	1617	7.4
5	**10b**	3.417	566	165.6
6	**10c**	20.1	1517	75.5
7	**Hydroxychloroquine**	29.25	356.4	12.2
8	**Chloroquine**	19.78	377.7	19.1
9	**Favipiravir**	1382	2633	1.9

[a] CC_{50} = Cytotoxic concentration due to 50% growth compared to the control experiment.
[b] IC_{50} = Inhibitory concentration due to 50% growth compared to the control experiment.
[c] SI (Selectivity index/therapeutical index) $= \frac{CC_{50}}{IC_{50}}$

*4.1.1. Reaction of 4-hydroxyacetophenone (**1**) and alkane sulfonylchloride **2a,b** (general procedure)*

A solution of equimolar amounts of the appropriate alkane sulfonylchlorides **2a,b** (5 mmol) in dry methylene chloride (5 ml) was added dropwise (10 min.) to the magnetically stirred solution of 4-hydroxyacetophenone **1** in methylene chloride (20 ml) containing triethylamine (5.5 mmol) at 0–5 °C. After complete addition, the reaction with stirred at the same conditions for 3 h and stored at room temperature (20–25 °C) overnight. The reaction mixture was washed with concentrated solution of $NaHCO_3$ (3 × 20 ml) then, with water. The solid separated upon evaporating the reaction mixture till dryness under reduced pressure, was crystallized from methanol affording the corresponding **3a,b** as colorless crystals.

*4.1.1.1. 4-Acetylphenyl methanesulfonate (**3a**)* [94]. It was obtained from the reaction of **1** and **2a** with mp 72–74 °C and yield 98% (1.05 g). IR: ν_{max}/cm^{-1} 1682, 1597, 1501. ^1H NMR (DMSO-d_6) δ (ppm): 2.61 (s, 3H, H_3CCO), 3.47 (s, 3H, H_3CS), 7.50 (d, J = 8.7 Hz, 2H, arom. H), 8.08 (d, J = 8.7 Hz, 2H, arom. H). ^{13}C NMR (DMSO-d_6) δ (ppm): 26.7 (H_3CCO), 37.7 (H_3CS), 122.3, 130.3, 135.5, 152.3 (arom. *C*), 196.8 (*CO*). Anal. Calcd. for $C_9H_{10}O_4S$ (214.24): C, 50.46; H, 4.71. Found: C, 50.65; H, 4.85.

*4.1.1.2. 4-Acetylphenyl ethanesulfonate (**3b**).* It was obtained from the reaction of **1** and **2b** with mp 63–65 °C and yield 89% (1.02 g). IR: ν_{max}/cm^{-1} 1678, 1593, 1497. ^1H NMR (DMSO-d_6) δ (ppm): 1.41 (t, J = 7.4 Hz, 3H, H_3CH_2CS), 2.60 (s, 3H, H_3CCO), 3.60 (q, J = 7.4 Hz, 2H, H_2CS), 7.48 (d, J = 8.7 Hz, 2H, arom. H), 8.07 (d, J = 8.7 Hz, 2H, arom. H). ^{13}C NMR (DMSO-d_6) δ (ppm): 8.0 (H_3CH_2CS), 26.7 (H_3CCO), 45.1 (H_2CS), 122.2, 130.4, 135.5, 152.2 (arom. *C*), 196.8 (*CO*). Anal. Calcd. for $C_{10}H_{12}O_4S$ (228.26): C, 52.62; H, 5.30. Found: C, 52.73; H, 5.46.

*4.1.2. Reaction of **3a,b** with **4a,b** (general procedure)*

A mixture of equimolar amounts of the appropriate isatin **4a,b** (5 mmol) and the corresponding acetophenone **3a,b** in ethanol absolute (15 ml) containing quantitative amount of diethylamine was stirred at room temperature (20–25 °C) for the appropriate time. The separated solid **5a-d** was collected washed with benzene (10 ml) and used in the

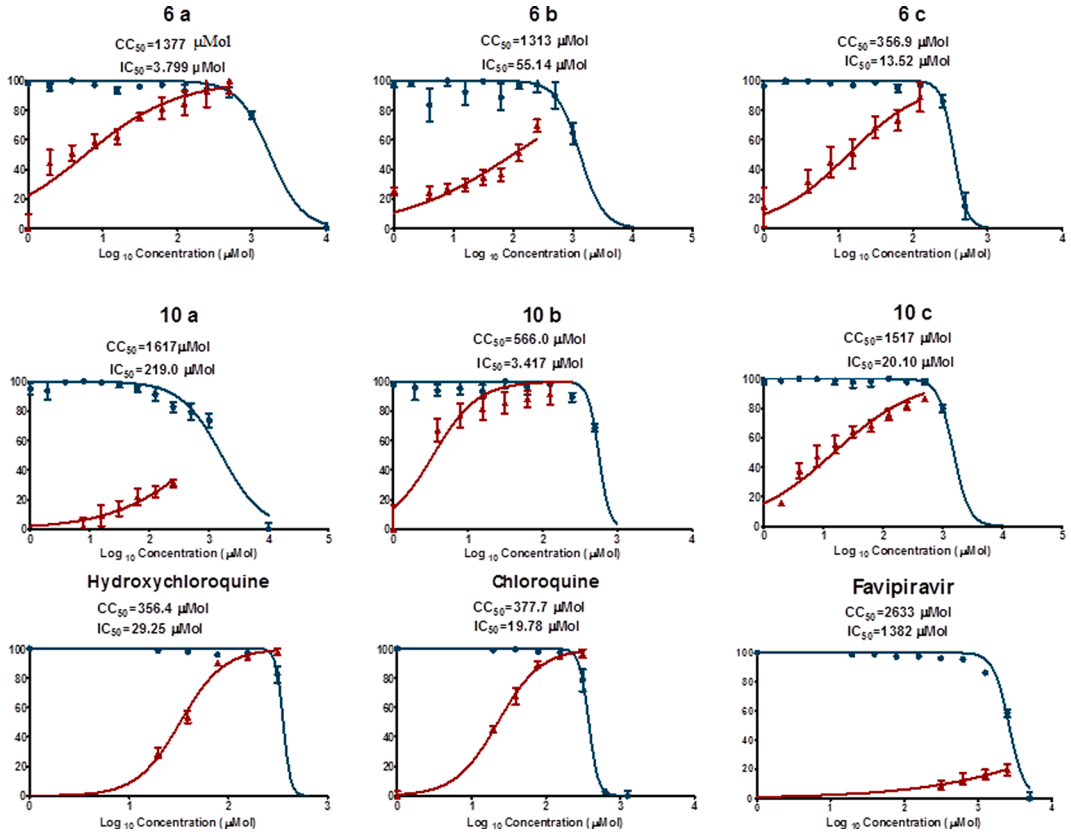

Fig. 9. Dose-response curves for the tested compounds against SARS-CoV-2.

Table 7
Molecular modeling results due to docking of compounds (**6a–c**, **10a–c**) and Sunitinib in the PDB ID: 4AGD and 3G0E responsible for VEGFR-2 and c-kit inhibitors, respectively.

Entry	Compd.	PDB ID: 4AGD		PDB ID: 3G0E	
		Docking score[a]	Docking observations	Docking score[a]	Docking observations
1	**6a**	−31.48	H-bond: indolyl CO - CYS919; π-σ interactions: indole - VAL848	−50.99	H-bond: indolyl CO - CYS673, indolyl NH - GLU671, sulfonyl SO-ASP677; π-σ interactions: indole–VAL603
2	**6b**	−40.07	H-bond: indolyl CO - CYS919, indolyl NH - GLU917	−50.69	H-bond: indolyl CO - CYS673, indolyl NH - GLU671; π-σ interactions: indole–VAL603
3	**6c**	−35.67	H-bond: indolyl CO - CYS919	−56.56	H-bond: indolyl CO - CYS673, indolyl NH - GLU671; π-σ interactions: indole–VAL603, phenyl-LEU595
4	**10a**	−34.67	H-bond: indolyl CO - CYS919, indolyl NH - GLU917	−57.88	H-bond: indolyl CO - CYS673, indolyl NH - GLU671, sulfonamide SO-ASP677; π-σ interactions: indole–VAL603
5	**10b**	−39.46	H-bond: indolyl CO - CYS919, indolyl NH - GLU917	−55.81	H-bond: indolyl CO - CYS673
6	**10c**	–33.29	H-bond: indolyl CO - CYS919, indolyl NH - GLU917	−58.33	H-bond: indolyl CO - CYS673, indolyl NH - GLU671, sulfonamide SO-ASP677
7	**Sunitinib**	−53.64	H-bond: indolyl CO - CYS919, indolyl NH - GLU917	−59.88	H-bond: indolyl CO - CYS673, indolyl NH - GLU671; π-σ interactions: indole–VAL603

[a] Docking score in kcal mol^{-1}.

next step without any more purification.

*4.1.2.1. 4-[2-(3-Hydroxy-2-oxoindolin-3-yl)acetyl]phenyl methanesulfonate (**5a**).* It was obtained from the reaction of **3a** and **4a** as colorless solid, reaction time 48 h, with mp 159–161 °C and yield 73% (1.31 g). IR: ν_{max}/cm^{-1} 3291, 1701, 1675, 1616, 1601. ^{1}H NMR (DMSO-d_6) δ (ppm): 3.44 (s, 3H, SCH_3), 3.61 (d, J = 17.5 Hz, 1H upfield H of CH_2CO), 4.09 (d, J = 17.5 Hz, 1H, downfield H of CH_2CO), 6.11 (s, 1H, OH), 6.82 (d, J = 7.7 Hz, 1H, arom. H), 6.87 (t, J = 7.4 Hz, 1H, arom. H), 7.17 (t, J = 7.6 Hz, 1H, arom. H), 7.29 (d, J = 7.3 Hz, 1H, arom. H), 7.47 (d, J = 8.7 Hz, 2H, arom. H), 8.02 (d, J = 8.7 Hz, 2H, arom. H), 10.29 (s, 1H, NH). ^{13}C NMR (DMSO-d_6) δ (ppm): 37.6 (SCH_3), 45.7 (CH_2CO), 72.9 (indolyl *C*-3), 109.3, 121.1, 122.3, 123.5, 128.9, 130.1, 131.5, 134.8, 142.8, 152.4 (arom. *C*), 178.2 [indolyl *C*O (*C*-2)], 195.4 (ketonic *C*O). Anal. Calcd. for $C_{17}H_{15}NO_6S$ (361.37): C, 56.50; H, 4.18; N, 3.88. Found: C, 56.59; H, 4.31; N, 4.02.

*4.1.2.2. 4-[2-(5-Chloro-3-hydroxy-2-oxoindolin-3-yl)acetyl]phenyl methanesulfonate (**5b**).* It was obtained from the reaction of **3a** and **4b** as colorless solid, reaction time 24 h, with mp 195–197 °C and yield 92% (1.82 g). IR: ν_{max}/cm^{-1} 3217, 1697, 1625, 1597. ^{1}H NMR (DMSO-d_6) δ (ppm): 3.45 (s, 3H, SCH_3), 3.67 (d, J = 17.9 Hz, 1H upfield H of CH_2CO), 4.18 (d, J = 17.9 Hz, 1H, downfield H of CH_2CO), 6.26 (s, 1H, OH), 6.85 (d, J = 8.3 Hz, 1H, arom. H), 7.23 (dd, J = 2.0, 8.2 Hz, 1H, arom. H), 7.41 (d, J = 1.8 Hz, 1H, arom. H), 7.49 (d, J = 8.6 Hz, 2H, arom. H), 8.03 (d, J = 8.7 Hz, 2H, arom. H), 10.44 (s, 1H, NH). ^{13}C NMR (DMSO-d_6) δ (ppm): 37.6 (SCH_3), 45.7 (CH_2CO), 73.0 (indolyl *C*-3), 110.8, 122.3, 123.9, 125.1, 128.6, 130.2, 133.7, 134.6, 141.8, 152.5 (arom. *C*), 177.9 [indolyl *C*O (*C*-2)], 195.5 (ketonic *C*O). Anal. Calcd. for $C_{17}H_{14}ClNO_6S$ (395.81): C, 51.59; H, 3.57; N, 3.54. Found: C, 51.79; H, 3.72; N, 3.70.

*4.1.2.3. 4-[2-(3-Hydroxy-2-oxoindolin-3-yl)acetyl]phenyl ethanesulfonate (**5c**).* It was obtained from the reaction of **3b** and **4a** as colorless solid, reaction time 24 h, with mp 156–158 °C and yield 80% (1.50 g). IR: ν_{max}/cm^{-1} 3306, 1709, 1678, 1618, 1601. ^{1}H NMR (DMSO-d_6) δ (ppm): 1.38 (t, J = 7.1 Hz, 3H, H_3CH_2CS), 3.58 (q, J = 7.1 Hz, 2H, SCH_2), 3.61 (d, J = 17.2 Hz, 1H upfield H of CH_2CO), 4.09 (d, J = 17.5 Hz, 1H, downfield H of CH_2CO), 6.12 (s, 1H, OH), 6.83 (d, J = 7.6 Hz, 1H, arom. H), 6.87 (t, J = 7.4 Hz, 1H, arom. H), 7.17 (t, J = 7.4 Hz, 1H, arom. H), 7.29 (d, J = 7.1 Hz, 1H, arom. H), 7.45 (d, J = 8.2 Hz, 2H, arom. H), 8.02 (d, J = 8.3 Hz, 2H, arom. H), 10.30 (s, 1H, NH). ^{13}C NMR (DMSO-d_6) δ (ppm): 8.1 (H_3CH_2CS), 45.1 (SCH_2), 45.9 (CH_2CO), 73.1 (indolyl *C*-3), 109.6, 121.3, 122.4, 123.7, 129.1, 130.3, 131.7, 134.9, 143.0, 152.4 (arom. *C*), 178.4 [indolyl *C*O (*C*-2)], 195.5 (ketonic *C*O). Anal. Calcd. for $C_{18}H_{17}NO_6S$ (375.40): C, 57.59; H, 4.56; N, 3.73. Found: C, 57.47; H, 4.75; N, 3.84.

*4.1.2.4. 4-[2-(5-Chloro-3-hydroxy-2-oxoindolin-3-yl)acetyl]phenyl ethanesulfonate (**5d**).* It was obtained from the reaction of **3b** and **4b** as colorless solid, reaction time 24 h, with mp 171–173 °C and yield 86% (1.75 g). IR: ν_{max}/cm^{-1} 3244, 1701, 1690, 1620, 1597. ^{1}H NMR (DMSO-d_6) δ (ppm): 1.39 (t, J = 7.3 Hz, 3H, H_3CH_2CS), 3.59 (q, J = 7.3 Hz, 2H, SCH_2), 3.68 (d, J = 17.9 Hz, 1H upfield H of CH_2CO), 4.19 (d, J = 17.9 Hz, 1H, downfield H of CH_2CO), 6.27 (s, 1H, OH), 6.86 (d, J = 8.3 Hz, 1H, arom. H), 7.24 (dd, J = 2.1, 8.3 Hz, 1H, arom. H), 7.42 (d, J = 2.0 Hz, 1H, arom. H), 7.47 (d, J = 8.7 Hz, 2H, arom. H), 8.03 (d, J = 8.7 Hz, 2H, arom. H), 10.45 (s, 1H, NH). ^{13}C NMR (DMSO-d_6) δ (ppm): 8.0 (H_3CH_2CS), 45.0 (SCH_2), 45.7 (CH_2CO), 73.0 (indolyl *C*-3), 110.8, 122.2, 124.0, 125.2, 128.6, 130.2, 133.8, 134.5, 141.8, 152.4 (arom. *C*), 177.9 [indolyl *C*O (*C*-2)], 195.4 (ketonic *C*O). Anal. Calcd. for $C_{18}H_{16}ClNO_6S$ (409.84): C, 52.75; H, 3.94; N, 3.42. Found: C, 52.88; H, 4.14; N, 3.54.

*4.1.3. Acidic dehydration of **5** (general procedure)*

Hydrochloric acid (25 ml, 25%) was added dropwise (10 min.) to a magnetically stirred solution of **5** (5 mmol) in absolute ethanol (12.5 ml) at room temperature (20–25 °C) for the appropriate time. The separated solid was collected, washed with water and purified by crystallization from a suitable solvent affording the corresponding **6a,b**; and chromatographic tool (silica gel TLC) giving **6c**.

*4.1.3.1. (E)-4-[2-(2-Oxoindolin-3-ylidene)acetyl]phenyl methanesulfonate (**6a**).* It was obtained from acidic dehydration of **5a** for 72 h as red microcrystals from *n*-butanol with mp 222–224 °C and yield 86% (1.47 g). IR: ν_{max}/cm^{-1} 3352, 1721, 1659, 1601. ^{1}H NMR (DMSO-d_6) δ (ppm): 3.51 (s, 3H, SCH_3), 6.91 (d, J = 7.8 Hz, 1H, arom. H), 6.98 (t, J = 7.7 Hz, 1H, arom. H), 7.37 (t, J = 7.7 Hz, 1H, arom. H), 7.59 (d, J = 8.6 Hz, 2H, arom. H), 7.74 (s, 1H, olefinic CH), 8.09 (d, J = 7.7 Hz, 1H, arom. H), 8.21 (d, J = 8.6 Hz, 2H, arom. H), 10.83 (s, 1H, NH). ^{13}C NMR (DMSO-d_6) δ (ppm): 37.8 (SCH_3), 110.3, 119.9, 121.7, 122.8, 125.3, 126.8, 130.8, 133.1, 135.8, 136.8, 145.0, 152.7 (arom. *C*), 168.1 [indolyl *C*O (*C*-2)], 190.0 (ketonic *C*O). Anal. Calcd. for $C_{17}H_{13}NO_5S$

(343.35): C, 59.47; H, 3.82; N, 4.08. Found: C, 59.29; H, 3.66 N, 3.95.

*4.1.3.2. (E)-4-[2-(2-Oxoindolin-3-ylidene)acetyl]phenyl ethanesulfonate (**6b**).* It was obtained from acidic dehydration of **5c** for 72 h as red microcrystals from methanol with mp 166–170 °C and yield 75% (1.34 g). IR: ν_{max}/cm^{-1} 3159, 1713, 1659, 1620. ^{1}H NMR (DMSO-d_6) δ (ppm): 1.41 (t, $J = 7.3$ Hz, 3H, CH_3), 3.63 (q, $J = 7.4$ Hz, 2H, SCH_2), 6.90 (d, $J =$ 7.8 Hz, 1H, arom. H), 6.97 (t, $J = 7.7$ Hz, 1H, arom. H), 7.36 (t, $J = 7.7$ Hz, 1H, arom. H), 7.55 (d, $J = 8.8$ Hz, 2H, arom. H), 7.72 (s, 1H, olefinic CH), 8.07 (d, $J = 7.8$ Hz, 1H, arom. H), 8.20 (d, $J = 8.7$ Hz, 2H, arom. H), 10.82 (s, 1H, NH). ^{13}C NMR (DMSO-d_6) δ (ppm): 8.0 (*C*H_3), 45.1 (*SC*H_2), 110.3, 119.8, 121.7, 122.6, 125.3, 126.8, 130.8, 133.0, 135.7, 136.7, 145.0, 152.6 (arom. *C*), 168.1 [indolyl *C*O (*C*-2)], 189.9 (ketonic *C*O). Anal. Calcd. for $C_{18}H_{15}NO_5S$ (357.38): C, 60.50; H, 4.23; N, 3.92. Found: C, 60.39H, 4.31; N, 3.73.

*4.1.3.3. (E)-4-[2-(5-Chloro-2-oxoindolin-3-ylidene)acetyl]phenyl ethanesulfonate (**6c**).* It was obtained from acidic dehydration of **5d** for 72 h as red microcrystals purified by silica gel TLC (60 G, F254 glass plate) using CH_2Cl_2 for elution, with mp 180–182 °C and yield 77% (1.51 g). IR: ν_{max}/cm^{-1} 3179, 1713, 1659, 1601. ^{1}H NMR (DMSO-d_6) δ (ppm): 1.41 (t, $J = 7.3$ Hz, 3H, CH_3), 3.64 (q, $J = 7.3$ Hz, 2H, SCH_2), 6.91 (d, $J = 8.3$ Hz, 1H, arom. H), 7.42 (dd, $J = 2.1$, 8.3 Hz, 1H, arom. H), 7.56 (d, $J =$ 8.7 Hz, 2H, arom. H), 7.80 (s, 1H, olefinic CH), 8.17 (d, $J = 1.9$ Hz, 1H, arom. H), 8.21 (d, $J = 8.7$ Hz, 2H, arom. H), 10.96 (s, 1H, NH). ^{13}C NMR (DMSO-d_6) δ (ppm): 8.0 (*C*H_3), 45.1 (*SC*H_2), 111.8, 121.3, 122.6, 125.5, 126.4, 131.0, 132.5, 135.6, 136.2, 143.9, 152.7 (arom. *C*), 167.8 [indolyl *C*O (*C*-2)], 189.5 (ketonic *C*O). Anal. Calcd. for $C_{18}H_{14}ClNO_5S$ (391.82): C, 55.18; H, 3.60; N, 3.57. Found: C, 55.33; H, 3.73; N, 3.51.

*4.1.4. Reaction of 4-aminoacetophenone (**7**) and alkane sulfonylchloride **2a-c** (general procedure)*

A solution of the appropriate alkane sulfonylchlorides **2a-c** (10 mmol in case of **2a,b** and 5 mmol in case of **2c**) in dry methylene chloride (5 ml) was added dropwise (10 min.) to the magnetically stirred solution of 4-aminoacetophenone **7** (5 mmol) in methylene chloride (20 ml) containing triethylamine (11 mmol in case of **2a,b** and 5.5 mmol in case of **2c**) at 0–5 °C. After complete addition, the reaction with stirred at the same conditions for 3 h and stored at room temperature (20–25 °C) overnight. The reaction mixture was washed with concentrated solution of $NaHCO_3$ (3 × 20 ml) then, with water. The solid separated upon evaporation the reaction mixture till dryness under reduced pressure, was collected and crystallized from a suitable solvent affording the corresponding **8a-c** as colorless crystals.

*4.1.4.1. N-(4-Acetylphenyl)-N-(methylsulfonyl)methanesulfonamide (**8a**).* It was obtained from the reaction of **7** and **2a** as colorless microcrystals from *n*-butanol with mp 172–174 °C and yield 82% (1.20 g). IR: ν_{max}/cm^{-1} 1682, 1597, 1504. ^{1}H NMR (DMSO-d_6) δ (ppm): 2.63 (s, 3H, H_3CCO), 3.57 (s, 6H, 2 SCH_3), 7.69 (d, $J = 8.5$ Hz, 2H, arom. H), 8.04 (d, $J = 8.4$ Hz, 2H, arom. H). ^{13}C NMR (DMSO-d_6) δ (ppm): 26.9 (H_3CCO), 43.1 (H_3CS), 129.1, 131.2, 137.7 (arom. *C*), 197.2 (*C*O). Anal. Calcd. for $C_{10}H_{13}NO_5S_2$ (291.34): C, 41.23; H, 4.50; N, 4.81. Found: C, 41.13; H, 4.43; N, 4.66.

*4.1.4.2. N-(4-Acetylphenyl)-N-(ethylsulfonyl)ethanesulfonamide (**8b**).* It was obtained from the reaction of **7** and **2b** as colorless microcrystals from benzene – pet. ether (60–80 °C) mixture as 1:3 v/v with mp 118–120 °C and yield 88% (1.40 g). IR: ν_{max}/cm^{-1} 1682, 1597, 1501. ^{1}H NMR (DMSO-d_6) δ (ppm): 1.36 (t, $J = 7.4$ Hz, 6H, 2 H_3CH_2CS), 2.63 (s, 3H, H_3CCO), 3.70 (q, $J = 7.3$ Hz, 4H, 2 SCH_2), 7.66 (d, $J = 8.3$ Hz, 2H, arom. H), 8.05 (d, $J = 8.3$ Hz, 2H, arom. H). ^{13}C NMR (DMSO-d_6) δ (ppm): 7.7 (H_3CH_2CS), 26.9 (H_3CCO), 49.9 (SCH_2), 129.2, 131.8, 137.7 (arom. *C*), 197.3 (*C*O). Anal. Calcd. for $C_{12}H_{17}NO_5S_2$ (319.39): C, 45.13; H, 5.37; N, 4.39. Found: C, 45.07; H, 5.40; N, 4.29.

*4.1.4.3. N-(4-Acetylphenyl)propane-1-sulfonamide (**8c**).* It was obtained from the reaction of **7** and **2c** as colorless microcrystals from methanol with mp 125–127 °C and yield 92% (1.11 g). IR: ν_{max}/cm^{-1} 3252, 3213, 1670, 1601, 1578. ^{1}H NMR (DMSO-d_6) δ (ppm): 0.94 (t, $J = 7.5$ Hz, 3H, $H_3CH_2CH_2CS$), 1.69 (sextet, $J = 7.4$ Hz, 2H, H_2CH_2CS), 2.52 (s, 3H, H_3CCO), 3.18 (t, $J = 7.6$ Hz, 2H, SCH_2), 7.30 (d, $J = 8.7$ Hz, 2H, arom. H), 7.93 (d, $J = 8.7$ Hz, 2H, arom. H), 10.33 (s, 1H, NH). ^{13}C NMR (DMSO-d_6) δ (ppm): 12.4 ($H_3CH_2CH_2CS$), 16.8 (H_2CH_2CS), 26.3 (H_3CCO), 52.8 (SCH_2), 117.3, 129.9, 131.5, 143.0 (arom. *C*), 196.4 (*C*O). Anal. Calcd. for $C_{11}H_{15}NO_3S$ (241.31): C, 54.75; H, 6.27; N, 5.80. Found: C, 54.58; H, 6.46; N, 5.74.

*4.1.5. Reaction of **8a-c** with **4a-c** (general procedure)*

A mixture of equimolar amounts of the appropriate isatin **4a-c** (5 mmol) and the corresponding acetophenone **8a-c** in ethanol absolute (15 ml) containing quantitative amount of diethylamine was stirred at room temperature (20–25 °C) for the appropriate time. The separated solid **9a–g** was collected washed with benzene (10 ml) and used in the next step without any more purification.

*4.1.5.1. N-{4-[2-(3-Hydroxy-2-oxoindolin-3-yl)acetyl]phenyl}-N-(methylsulfonyl)methanesulfonamide (**9a**).* It was obtained from the reaction of **8a** and **4a** as colorless solid, reaction time 48 h, with mp 209–211 °C and yield 72% (1.57 g). IR: ν_{max}/cm^{-1} 3410, 1701, 1682, 1620, 1601. ^{1}H NMR (DMSO-d_6) δ (ppm): 3.56 (s, 6H, 2 SCH_3), 3.63 (d, $J = 17.6$ Hz, 1H upfield H of CH_2CO), 4.11 (d, $J = 17.6$ Hz, 1H, downfield H of CH_2CO), 6.10 (s, 1H, OH), 6.82 (d, $J = 7.7$ Hz, 1H, arom. H), 6.86 (t, $J = 7.5$ Hz, 1H, arom. H), 7.17 (t, $J = 7.7$ Hz, 1H, arom. H), 7.29 (d, $J = 7.3$ Hz, 1H, arom. H), 7.66 (d, $J = 8.4$ Hz, 2H, arom. H), 7.99 (d, $J = 8.4$ Hz, 2H, arom. H), 10.29 (s, 1H, NH). ^{13}C NMR (DMSO-d_6) δ (ppm): 43.0 (SCH_3), 45.8 (CH_2CO), 72.9 (indolyl *C*-3), 109.3, 121.1, 123.6, 128.9, 129.0, 131.2, 131.5, 137.0, 137.9, 142.8 (arom. *C*), 178.1 [indolyl *C*O (*C*-2)], 195.8 (ketonic *C*O). Anal. Calcd. for $C_{18}H_{18}N_2O_7S_2$ (438.47): C, 49.31; H, 4.14; N, 6.39. Found: C, 49.51; H, 4.28; N, 6.55.

*4.1.5.2. N-{4-[2-(5-Chloro-3-hydroxy-2-oxoindolin-3-yl)acetyl]phenyl}-N-(methylsulfonyl)methanesulfonamide (**9b**).* It was obtained from the reaction of **8a** and **4b** as colorless solid, reaction time 72 h, with mp 208–210 °C and yield 69% (1.64 g). IR: ν_{max}/cm^{-1} 3337, 1724, 1694, 1621, 1601. ^{1}H NMR (DMSO-d_6) δ (ppm): 3.57 (s, 6H, 2 SCH_3), 3.70 (d, $J = 18.0$ Hz, 1H upfield H of CH_2CO), 4.21 (d, $J = 18.1$ Hz, 1H, downfield H of CH_2CO), 6.26 (s, 1H, OH), 6.85 (d, $J = 8.3$ Hz, 1H, arom. H), 7.24 (dd, $J = 2.1$, 8.3 Hz, 1H, arom. H), 7.42 (d, $J = 2.1$ Hz, 1H, arom. H), 7.69 (d, $J = 8.5$ Hz, 2H, arom. H), 8.00 (d, $J = 8.5$ Hz, 2H, arom. H), 10.44 (s, 1H, NH). ^{13}C NMR (DMSO-d_6) δ (ppm): 43.1 (SCH_3), 45.7 (CH_2CO), 72.9 (indolyl *C*-3), 110.7, 117.3, 123.9, 125.1, 128.6, 129.0, 129.7, 131.2, 133.7, 136.8, 138.0, 141.8 (arom. *C*), 177.9 [indolyl *C*O (*C*-2)], 195.9 (ketonic *C*O). Anal. Calcd. for $C_{18}H_{17}ClN_2O_7S_2$ (472.91): C, 45.72; H, 3.62; N, 5.92. Found: C, 45.81; H, 3.78; N, 6.06.

*4.1.5.3. N-(Ethylsulfonyl)-N-{4-[2-(3-hydroxy-2-oxoindolin-3-yl)acetyl]phenyl}ethanesulfonamide (**9c**).* It was obtained from the reaction of **8b** and **4a** as colorless solid, reaction time 48 h, with mp 204–206 °C and yield 67% (1.56 g). IR: ν_{max}/cm^{-1} 3402, 3198, 1697, 1682, 1620, 1601. ^{1}H NMR (DMSO-d_6) δ (ppm): 1.34 (t, $J = 7.3$ Hz, 6H, 2 CH_3), 3.63 (d, $J =$ 17.6 Hz, 1H, upfield H of CH_2CO), 3.68 (q, $J = 7.4$ Hz, 4H, 2 SCH_2), 4.12 (d, $J = 17.6$ Hz, 1H, downfield H of CH_2CO), 6.12 (s, 1H, OH), 6.84 (d, J = 7.7 Hz, 1H, arom. H), 6.88 (t, $J = 7.5$ Hz, 1H, arom. H), 7.18 (t, $J = 7.7$ Hz, 1H, arom. H), 7.31 (d, $J = 7.3$ Hz, 1H, arom. H), 7.63 (d, $J = 8.5$ Hz, 2H, arom. H), 8.00 (d, $J = 8.4$ Hz, 2H, arom. H), 10.30 (s, 1H, NH). ^{13}C NMR (DMSO-d_6) δ (ppm): 7.6 (CH_3), 45.8 (CH_2CO), 49.8 (SCH_2), 72.9 (indolyl *C*-3), 109.3, 121.1, 123.6, 128.9, 131.5, 131.7, 137.0, 137.7, 142.8 (arom. *C*), 178.1 [indolyl *C*O (*C*-2)], 195.8 (ketonic *C*O). Anal. Calcd. for $C_{20}H_{22}N_2O_7S_2$ (466.52): C, 51.49; H, 4.75; N, 6.00. Found: C, 51.60; H, 4.82; N, 6.05.

*4.1.5.4. N-{4-[2-(5-Chloro-3-hydroxy-2-oxoindolin-3-yl)acetyl]phenyl}-N-(ethylsulfonyl)ethanesulfonamide (**9d**).* It was obtained from the reaction of **8b** and **4b** as colorless solid, reaction time 72 h, with mp 191–193 °C and yield 66% (1.66 g). IR: ν_{max}/cm^{-1} 3252, 1695, 1682, 1620, 1601. ^{1}H NMR (DMSO-d_6) δ (ppm): 1.34 (t, J = 7.3 Hz, 6H, 2 CH_3), 3.66–3.71 (m, 5H, 2 SCH_2 + upfield H of CH_2CO), 4.20 (d, J = 18.0 Hz, 1H, downfield H of CH_2CO), 6.27 (s, 1H, OH), 6.85 (d, J = 8.2 Hz, 1H, arom. H), 7.24 (dd, J = 1.6, 8.2 Hz, 1H, arom. H), 7.42 (d, J = 1.1 Hz, 1H, arom. H), 7.64 (d, J = 8.3 Hz, 2H, arom. H), 8.00 (d, J = 8.3 Hz, 2H, arom. H), 10.45 (s, 1H, NH). ^{13}C NMR (DMSO-d_6) δ (ppm): 7.7 (*C*H_3), 45.8 (*C*H_2CO), 49.9 (*SC*H_2), 73.0 (indolyl *C*-3), 110.8, 124.0, 125.2, 128.7, 129.0, 131.8, 133.8, 136.8, 138.0, 141.9 (arom. *C*), 178.0 [indolyl *CO* (*C*-2)], 196.0 (ketonic *CO*). Anal. Calcd. for $C_{20}H_{21}ClN_2O_7S_2$ (500.97): C, 47.95; H, 4.23; N, 5.59. Found: C, 48.13; H, 4.36; N, 5.78.

*4.1.5.5. N-{4-[2-(3-Hydroxy-2-oxoindolin-3-yl)acetyl]phenyl}-N-(propylsulfonyl)propane-1-sulfonamide (**9e**).* It was obtained from the reaction of **8c** and **4a** as colorless solid, reaction time 48 h, with mp 191–193 °C and yield 39% (0.96 g). IR: ν_{max}/cm^{-1} 3422, 3256, 1740, 1678, 1624, 1601. ^{1}H NMR (DMSO-d_6) δ (ppm): 1.00 (t, J = 7.4 Hz, 6H, 2 CH_3), 1.80 (sextet, J = 7.4 Hz, 4H, 2 SCH_2CH_2), 3.61 (d, J = 17.9 Hz, 1H upfield H of CH_2CO), 3.65 (t, J = 7.6 Hz, 4H, 2 SCH_2), 4.10 (d, J = 17.7 Hz, 1H, downfield H of CH_2CO), 6.09 (s, 1H, OH), 6.82 (d, J = 7.7 Hz, 1H, arom. H), 6.86 (t, J = 7.5 Hz, 1H, arom. H), 7.17 (t, J = 7.6 Hz, 1H, arom. H), 7.29 (d, J = 7.2 Hz, 1H, arom. H), 7.61 (d, J = 8.4 Hz, 2H, arom. H), 7.98 (d, J = 8.4 Hz, 2H, arom. H), 10.28 (s, 1H, NH). ^{13}C NMR (DMSO-d_6) δ (ppm): 12.4 (*C*H_3), 16.5 (SCH_2CH_2), 45.8 (*C*H_2CO), 56.6 (*SC*H_2), 72.9 (indolyl *C*-3), 109.3, 121.0, 123.6, 128.9, 131.5, 131.7, 137.0, 137.7, 142.8 (arom. *C*), 178.1 [indolyl *CO* (*C*-2)], 195.8 (ketonic *CO*). Anal. Calcd. for $C_{22}H_{26}N_2O_7S_2$ (494.58): C, 53.43; H, 5.30; N, 5.66. Found: C, 53.24; H, 5.41; N, 5.72.

*4.1.5.6. N-{4-[2-(5-Chloro-3-hydroxy-2-oxoindolin-3-yl)acetyl]phenyl}-N-(propylsulfonyl)propane-1-sulfonamide (**9f**).* It was obtained from the reaction of **8c** and **4b** as colorless solid, reaction time 72 h, with mp 179–181 °C and yield 46% (1.21 g). IR: ν_{max}/cm^{-1} 3356, 3256, 1721, 1682, 1620, 1601. ^{1}H NMR (DMSO-d_6) δ (ppm): 1.02 (t, J = 7.4 Hz, 6H, 2 CH_3), 1.83 (sextet, J = 7.4 Hz, 4H, 2 SCH_2CH_2), 3.67 (t, J = 7.7 Hz, 4H, 2 SCH_2), 3.71 (d, J = 18.9 Hz, 1H upfield H of CH_2CO), 4.22 (d, J = 18.0 Hz, 1H, downfield H of CH_2CO), 6.28 (s, 1H, OH), 6.87 (d, J = 8.3 Hz, 1H, arom. H), 7.25 (dd, J = 1.9, 8.3 Hz, 1H, arom. H), 7.43 (br s, 1H, arom. H), 7.65 (d, J = 8.4 Hz, 2H, arom. H), 8.01 (d, J = 8.4 Hz, 2H, arom. H), 10.46 (s, 1H, NH). ^{13}C NMR (DMSO-d_6) δ (ppm): 13.0 (*C*H_3), 17.1 (SCH_2CH_2), 46.3 (*C*H_2CO), 57.2 (*SC*H_2), 73.5 (indolyl *C*-3), 111.3, 124.5, 125.7, 128.8, 129.2, 129.5, 132.3, 134.3, 137.3, 138.4, 142.4 (arom. *C*), 178.4 [indolyl *CO* (*C*-2)], 196.4 (ketonic *CO*). Anal. Calcd. for $C_{22}H_{25}ClN_2O_7S_2$ (529.02): C, 49.95; H, 4.76; N, 5.30. Found: C, 50.08; H, 4.92; N, 5.39.

*4.1.5.7. N-{4-[2-(3-Hydroxy-5-methoxy-2-oxoindolin-3-yl)acetyl]phenyl}-N-(propylsulfonyl)propane-1-sulfonamide (**9 g**).* It was obtained from the reaction of **8c** and **4c** as colorless solid, reaction time 72 h, with mp 161–163 °C and yield 44% (1.14 g). IR: ν_{max}/cm^{-1} 3348, 1717, 1686, 1605. ^{1}H NMR (DMSO-d_6) δ (ppm): 1.02 (t, J = 7.4 Hz, 6H, 2 CH_3), 1.82 (sextet, J = 7.3 Hz, 4H, 2 SCH_2CH_2), 3.60–3.68 (m, 8H, 2 SCH_2 + OCH_3 + upfield H of CH_2CO), 4.12 (d, J = 17.6 Hz, 1H, downfield H of CH_2CO), 6.12 (s, 1H, OH), 6.75 (br s, 2H, arom. H), 7.00 (br s, 1H, arom. H), 7.64 (d, J = 8.3 Hz, 2H, arom. H), 8.00 (d, J = 8.3 Hz, 2H, arom. H), 10.13 (s, 1H, NH). ^{13}C NMR (DMSO-d_6) δ (ppm): 12.4 (*C*H_3), 16.5 (SCH_2CH_2), 45.8 (*C*H_2CO), 55.3 (OCH_3), 56.6 (*SC*H_2), 73.4 (indolyl *C*-3), 109.6, 110.9, 113.3, 128.9, 131.7, 132.8, 136.0, 137.0, 137.7, 154.6 (arom. *C*), 178.1 [indolyl *CO* (*C*-2)], 195.8 (ketonic *CO*). Anal. Calcd. for $C_{23}H_{28}N_2O_8S_2$ (524.60): C, 52.66; H, 5.38; N, 5.34. Found: C, 52.82; H, 5.46; N, 5.51.

*4.1.6. Acidic dehydration of **9** (general procedure)*

Hydrochloric acid (25 ml, 25%) was added dropwise (10 min.) to a magnetically stirred solution of **9** (5 mmol) in absolute ethanol (12.5 ml) at room temperature (20–25 °C) for the appropriate time. The separated solid was collected, washed with water and crystallized from a suitable solvent affording the corresponding **10**.

*4.1.6.1. (E)-N-(Methylsulfonyl)-N-{4-[2-(2-oxoindolin-3-ylidene)acetyl]phenyl}methanesulfonamide (**10a**).* It was obtained from acidic dehydration of **9a** for 72 h as red microcrystals from methanol with mp 239–241 °C and yield 66% (1.39 g). IR: ν_{max}/cm^{-1} 3194, 1717, 1663, 1505. ^{1}H NMR (DMSO-d_6) δ (ppm): 3.61 (s, 6H, 2 SCH_3), 6.91 (d, J = 7.8 Hz, 1H, arom. H), 6.98 (t, J = 7.7 Hz, 1H, arom. H), 7.37 (t, J = 7.7 Hz, 1H, arom. H), 7.75 (s, 1H, olefinic CH), 7.79 (d, J = 8.5 Hz, 2H, arom. H), 8.11 (d, J = 7.7 Hz, 1H, arom. H), 8.18 (d, J = 8.5 Hz, 2H, arom. H), 10.83 (s, 1H, NH). ^{13}C NMR (DMSO-d_6) δ (ppm): 43.1 (*SC*H_3), 110.3, 119.8, 121.7, 125.3, 126.8, 129.6, 131.6, 133.1, 137.0, 138.16, 138.23, 145.1 (arom. *C* + olefinic *C*), 168.1 [indolyl *CO* (*C*-2)], 190.4 (ketonic *CO*). Anal. Calcd. for $C_{18}H_{16}N_2O_6S_2$ (420.45): C, 51.42; H, 3.84; N, 6.66. Found: C, 51.31; H, 3.71; N, 6.56.

*4.1.6.2. (E)-N-(Ethylsulfonyl)-N-{4-[2-(2-oxoindolin-3-ylidene)acetyl]phenyl}ethanesulfonamide (**10b**).* It was obtained from acidic dehydration of **9c** for 72 h as red microcrystals from methanol with mp 220–222 °C and yield 70% (1.56 g). IR: ν_{max}/cm^{-1} 3395, 3159, 1717, 1663, 1605. ^{1}H NMR (DMSO-d_6) δ (ppm): 1.36 (t, J = 7.4 Hz, 6H, 2 CH_3), 3.71 (q, J = 7.4 Hz, 4H, 2 SCH_2), 6.90 (d, J = 7.8 Hz, 1H, arom. H), 6.98 (t, J = 7.6 Hz, 1H, arom. H), 7.37 (t, J = 7.7 Hz, 1H, arom. H), 7.73 (d, J = 7.8 Hz, 2H, arom. H), 7.74 (s, 1H, olefinic CH), 8.10 (d, J = 7.7 Hz, 1H, arom. H), 8.17 (d, J = 8.5 Hz, 2H, arom. H), 10.83 (s, 1H, NH). ^{13}C NMR (DMSO-d_6) δ (ppm): 7.6 (*C*H_3), 49.9 (*SC*H_2), 110.3, 119.8, 121.7, 125.3, 126.8, 129.5, 132.1, 133.2, 136.9, 138.1, 145.1 (arom. *C* + olefinic *C*), 168.1 [indolyl *CO* (*C*-2)], 190.3 (ketonic *CO*). Anal. Calcd. for $C_{20}H_{20}N_2O_6S_2$ (448.51): C, 53.56; H, 4.49; N, 6.25. Found: C, 53.42; H, 4.42; N, 6.11.

*4.1.6.3. (E)-N-{4-[2-(5-Chloro-2-oxoindolin-3-ylidene)acetyl]phenyl}-N-(ethylsulfonyl)ethanesulfonamide (**10c**).* It was obtained from acidic dehydration of **9d** for 72 h as red microcrystals from methanol with mp 222–224 °C and yield 77% (1.85 g). IR: ν_{max}/cm^{-1} 3171, 1717, 1663, 1601. ^{1}H NMR (DMSO-d_6) δ (ppm): 1.37 (t, J = 7.3 Hz, 6H, 2 CH_3), 3.72 (q, J = 7.2 Hz, 4H, 2 SCH_2), 6.89 (d, J = 8.3 Hz, 1H, arom. H), 7.40 (dd, J = 1.6, 8.3 Hz, 1H, arom. H), 7.74 (d, J = 8.3 Hz, 2H, arom. H), 7.80 (s, 1H, olefinic CH), 8.18 (d, J = 8.6 Hz, 2H, arom. H), 8.19 (d, J = 2.0 Hz, 1H, arom. H), 10.95 (s, 1H, NH). ^{13}C NMR (DMSO-d_6) δ (ppm): 7.6 (*C*H_3), 49.9 (*SC*H_2), 111.8, 121.3, 125.6, 126.3, 126.5, 129.6, 132.1, 132.6, 136.4, 138.1, 138.2, 144.0 (arom. *C* + olefinic *C*), 167.8 [indolyl *CO* (*C*-2)], 189.9 (ketonic *CO*). Anal. Calcd. for $C_{20}H_{19}ClN_2O_6S_2$ (482.95): C, 49.74; H, 3.97; N, 5.80. Found: C, 49.55; H, 3.86; N, 5.73.

*4.1.7. Reaction of **4a-e** with **11a,b** (general procedure)*

A mixture of equimolar amounts of the appropriate isatin **4a-e** (5 mmol) and the corresponding 2-acetylbenzimidazole **11a,b** [95,96] in ethanol absolute (15 ml) containing quantitative amount of diethylamine was stirred at room temperature (20–25 °C) for 3 h. The reaction mixture was stored at room temperature overnight, the separated solid **12a–h** was collected washed with benzene (10 ml) and used in the next step without any more purification.

*4.1.7.1. 3-Hydroxy-3-[2-(1-methyl-1H-benzo[d]imidazol-2-yl)-2-oxoethyl]indolin-2-one (**12a**).* It was obtained from the reaction of **4a** and **11a** as colorless solid with mp 139–141 °C and yield 84% (1.35 g). IR: ν_{max}/cm^{-1} 3568, 3302, 3213, 1709, 1690, 1678, 1628, 1612. ^{1}H NMR (DMSO-d_6) δ (ppm): 3.73 (d, J = 17.1 Hz, 1H upfield H of CH_2CO), 3.84 (s, 3H, NCH_3), 4.36 (d, J = 17.1 Hz, 1H, downfield H of CH_2CO),

6.29 (s, 1H, OH), 6.85 (t, $J = 7.8$ Hz, 2H, arom. H), 7.17 (t, $J = 7.5$ Hz, 1H, arom. H), 7.30 (d, $J = 7.2$ Hz, 1H, arom. H), 7.34 (t, $J = 7.6$ Hz, 1H, arom. H), 7.41 (t, $J = 7.6$ Hz, 1H, arom. H), 7.61 (d, $J = 8.1$ Hz, 1H, arom. H), 7.83 (d, $J = 8.1$ Hz, 1H, arom. H), 10.36 (s, 1H, NH). ^{13}C NMR (DMSO-d_6) δ (ppm): 31.9 (NCH_3), 46.8 (CH_2CO), 73.2 (indolyl *C*-3) 109.6, 111.6, 121.2, 121.4, 123.6, 123.9, 125.8, 129.2, 131.4, 136.7, 140.8, 142.7, 145.6 (arom. *C*), 178.1 [indolyl *CO* (*C*-2)], 191.3 (ketonic *CO*). Anal. Calcd. for $C_{18}H_{15}N_3O_3$ (321.34): C, 67.28; H, 4.71; N, 13.08. Found: C, 67.18; H, 4.57; N, 12.92.

*4.1.7.2. 3-[2-(1-Ethyl-1H-benzo[d]imidazol-2-yl)-2-oxoethyl]-3-hydroxyindolin-2-one (**12b**).* It was obtained from the reaction of **4a** and **11b** as colorless solid with mp 134–136 °C and yield 74% (1.24 g). IR: ν_{max}/cm^{-1} 3595, 3306, 3213, 1710, 1690, 1686, 1624. ^{1}H NMR (DMSO-d_6) δ (ppm): 1.09 (t, $J = 6.6$ Hz, 3H, CH_3), 3.69 (d, $J = 16.6$ Hz, 1H upfield H of CH_2CO), 4.38 (br d, 3H, NCH_2CH_3 + downfield H of CH_2CO), 6.29 (s, 1H, OH), 6.82–6.83 (m, 2H, arom. H), 7.15 (t, $J = 7.5$ Hz, 1H, arom. H), 7.27 (d, $J = 7.0$ Hz, 1H, arom. H), 7.35 (t, $J = 7.3$ Hz, 1H, arom. H), 7.43 (t, $J = 7.3$ Hz, 1H, arom. H), 7.66 (d, $J = 8.2$ Hz, 1H, arom. H), 7.85 (d, $J = 8.1$ Hz, 1H, arom. H), 10.35 (s, 1H, NH). ^{13}C NMR (DMSO-d_6) δ (ppm): 15.2 (CH_3), 39.8 (NCH_2CH_3), 46.7 (CH_2CO), 73.3 (indolyl *C*-3) 109.6, 111.5, 121.3, 121.4, 123.7, 123.9, 125.9, 129.2, 131.2, 135.8, 141.0, 142.6, 145.1 (arom. *C*), 178.1 [indolyl *CO* (*C*-2)], 191.3 (ketonic *CO*). Anal. Calcd. for $C_{19}H_{17}N_3O_3$ (335.36): C, 68.05; H, 5.11; N, 12.53. Found: C, 68.21; H, 5.02; N, 12.67.

*4.1.7.3. 5-Chloro-3-hydroxy-3-[2-(1-methyl-1H-benzo[d]imidazol-2-yl)-2-oxoethyl]indolin-2-one (**12c**).* It was obtained from the reaction of **4b** and **11a** as colorless solid with mp 186–188 °C and yield 71% (1.26 g). IR: ν_{max}/cm^{-1} 3348, 3298, 1717, 1686, 1670, 1624. ^{1}H NMR (DMSO-d_6) δ (ppm): 3.82 (d, $J = 17.7$ Hz, 1H upfield H of CH_2CO), 3.88 (s, 3H, NCH_3), 4.36 (d, $J = 17.6$ Hz, 1H, downfield H of CH_2CO), 6.39 (s, 1H, OH), 6.85 (d, $J = 8.2$ Hz, 1H, arom. H), 7.23 (d, $J = 8.1$ Hz, 1H, arom. H), 7.35 (t, $J = 7.4$ Hz, 1H, arom. H), 7.40–7.44 (m, 2H, arom. H), 7.64 (d, $J = 8.1$ Hz, 1H, arom. H), 7.84 (d, $J = 8.1$ Hz, 1H, arom. H), 10.50 (s, 1H, NH). ^{13}C NMR (DMSO-d_6) δ (ppm): 32.0 (NCH_3), 46.7 (CH_2CO), 73.1 (indolyl *C*-3) 111.0, 111.6, 121.2, 123.6, 124.3, 125.4, 125.8, 128.9, 133.5, 136.7, 140.8, 141.6, 145.4 (arom. *C*), 177.8 [indolyl *CO* (*C*-2)], 191.3 (ketonic *CO*). Anal. Calcd. for $C_{18}H_{14}ClN_3O_3$ (355.78): C, 60.77; H, 3.97; N, 11.81. Found: C, 61.06; H, 4.09; N, 11.99.

*4.1.7.4. 5-Chloro-3-[2-(1-ethyl-1H-benzo[d]imidazol-2-yl)-2-oxoethyl]-3-hydroxyindolin-2-one (**12d**).* It was obtained from the reaction of **4b** and **11b** as colorless solid with mp 169–171 °C and yield 75% (1.38 g). IR: ν_{max}/cm^{-1} 3464, 3256, 1740, 1701, 1686, 1620. ^{1}H NMR (DMSO-d_6) δ (ppm): 1.13 (t, $J = 6.5$ Hz, 3H, CH_3), 3.80 (d, $J = 17.2$ Hz, 1H upfield H of CH_2CO), 4.35–4.41 (m, 3H, NCH_2CH_3 + downfield H of CH_2CO), 6.41 (s, 1H, OH), 6.84 (d, $J = 8.1$ Hz, 1H, arom. H), 7.22 (d, $J = 8.2$ Hz, 1H, arom. H), 7.34–7.38 (m, 2H, arom. H), 7.43 (t, $J = 7.3$ Hz, 1H, arom. H), 7.67 (d, $J = 8.1$ Hz, 1H, arom. H), 7.86 (d, $J = 8.1$ Hz, 1H, arom. H), 10.50 (s, 1H, NH). ^{13}C NMR (DMSO-d_6) δ (ppm): 15.2 (CH_3), 39.8 (NCH_2CH_3), 46.7 (CH_2CO), 73.3 (indolyl *C*-3) 111.0, 111.5, 121.4, 123.7, 124.3, 125.4, 125.9, 128.9, 133.4, 135.7, 141.0, 141.6, 144.9 (arom. *C*), 177.8 [indolyl *CO* (*C*-2)], 191.2 (ketonic *CO*). Anal. Calcd. for $C_{19}H_{16}ClN_3O_3$ (369.81): C, 61.71; H, 4.36; N, 11.36. Found: C, 61.85; H, 4.42; N, 11.45.

*4.1.7.5. 3-Hydroxy-5-methoxy-3-[2-(1-methyl-1H-benzo[d]imidazol-2-yl)-2-oxoethyl]indolin-2-one (**12e**).* It was obtained from the reaction of **4c** and **11a** as colorless solid with mp 174–176 °C and yield 78% (1.37 g). IR: ν_{max}/cm^{-1} 3186, 1724, 1686, 1655, 1612. ^{1}H NMR (DMSO-d_6) δ (ppm): 3.57 (s, 3H, OCH_3), 3.71 (d, $J = 16.9$ Hz, 1H upfield H of CH_2CO), 3.86 (s, 3H, NCH_3), 4.33 (d, $J = 16.9$ Hz, 1H, downfield H of CH_2CO), 6.27 (s, 1H, OH), 6.73 (s, 2H, arom. H), 6.94 (s, 1H, arom. H), 7.35 (t, $J = 7.0$ Hz, 1H, arom. H), 7.43 (t, $J = 7.2$ Hz, 1H, arom. H), 7.63 (d, $J = 8.0$ Hz, 1H, arom. H), 7.84 (d, $J = 8.0$ Hz, 1H, arom. H), 10.17 (s, 1H, NH). ^{13}C NMR (DMSO-d_6) δ (ppm): 31.9 (NCH_3), 46.8 (CH_2CO), 55.3 (OCH_3), 73.6 (indolyl *C*-3) 109.9, 111.0, 111.5, 113.7, 121.2, 123.6, 125.7, 132.4, 135.8, 136.7, 140.8, 145.7, 154.6 (arom. *C*), 178.0 [indolyl *CO* (*C*-2)], 191.3 (ketonic *CO*). Anal. Calcd. for $C_{19}H_{17}N_3O_4$ (351.36): C, 64.95; H, 4.88; N, 11.96. Found: C, 65.13; H, 5.01; N, 12.07.

*4.1.7.6. 3-[2-(1-Ethyl-1H-benzo[d]imidazol-2-yl)-2-oxoethyl]-3-hydroxy-5-methoxyindolin-2-one (**12f**).* It was obtained from the reaction of **4c** and **11b** as colorless solid with mp 179–181 °C and yield 89% (1.62 g). IR: ν_{max}/cm^{-1} 3422, 3167, 1709, 1682, 1639. ^{1}H NMR (DMSO-d_6) δ (ppm): 1.11 (t, $J = 6.3$ Hz, 3H, CH_3), 3.54 (s, 3H, OCH_3), 3.67 (d, $J = 16.3$ Hz, 1H upfield H of CH_2CO), 4.33–4.42 (m, 3H, NCH_2CH_3 + downfield H of CH_2CO), 6.29 (s, 1H, OH), 6.72 (s, 2H, arom. H), 6.91 (s, 1H, arom. H), 7.36 (t, $J = 7.2$ Hz, 1H, arom. H), 7.43 (t, $J = 7.2$ Hz, 1H, arom. H), 7.67 (d, $J = 8.0$ Hz, 1H, arom. H), 7.86 (d, $J = 8.0$ Hz, 1H, arom. H), 10.17 (s, 1H, NH). ^{13}C NMR (DMSO-d_6) δ (ppm): 15.1 (CH_3), 39.7 (NCH_2CH_3), 46.7 (CH_2CO), 55.3 (OCH_3), 73.8 (indolyl *C*-3) 109.9, 111.0, 111.5, 113.9, 121.3, 123.6, 125.8, 132.3, 135.7, 141.0, 145.2, 154.6 (arom. *C*), 177.9 [indolyl *CO* (*C*-2)], 191.2 (ketonic *CO*). Anal. Calcd. for $C_{20}H_{19}N_3O_4$ (365.39): C, 65.74; H, 5.24; N, 11.50. Found: C, 65.81; H, 5.33; N, 11.68.

*4.1.7.7. 3-Hydroxy-3-[2-(1-methyl-1H-benzo[d]imidazol-2-yl)-2-oxoethyl]-1-(piperidin-1-ylmethyl)indolin-2-one (**12 g**).* It was obtained from the reaction of **4d** [97] and **11a** as colorless solid with mp 147–149 °C and yield 75% (1.57 g). IR: ν_{max}/cm^{-1} 3321, 1701, 1686, 1616. ^{1}H NMR (DMSO-d_6) δ (ppm): 1.36 (br s, 2H, piperidinyl H_2C-4), 1.47 (br s, 4H, piperidinyl H_2C-3/5), 2.57 (br d, 4H, piperidinyl H_2C-2/6), 3.79 (d, $J = 17.1$ Hz, 1H upfield H of CH_2CO), 3.84 (s, 3H, NCH_3), 4.37–4.40 (m, 3H, NCH_2N + downfield H of CH_2CO), 6.37 (s, 1H, OH), 6.92 (t, $J = 6.9$ Hz, 1H, arom. H), 7.11 (d, $J = 7.4$ Hz, 1H, arom. H), 7.24 (t, $J = 7.3$ Hz, 1H, arom. H), 7.35 (br s, 2H, arom. H), 7.42 (t, $J = 7.3$ Hz, 1H, arom. H), 7.62 (d, $J = 7.9$ Hz, 1H, arom. H), 7.83 (d, $J = 7.8$ Hz, 1H, arom. H). ^{13}C NMR (DMSO-d_6) δ (ppm): 23.8 (piperidinyl *C*-4), 25.4 (piperidinyl *C*-3/5), 31.8 (NCH_3), 47.0 (CH_2CO), 51.3 (piperidinyl *C*-2/6), 62.1 (NCH_2N), 72.9 (indolyl *C*-3), 109.9, 111.5, 121.2, 121.9, 123.4, 123.5, 125.7, 129.1, 130.4, 136.7, 140.8, 144.2, 145.5 (arom. *C*), 177.4 [indolyl *CO* (*C*-2)], 191.1 (ketonic *CO*). Anal. Calcd. for $C_{24}H_{26}N_4O_3$ (418.50): C, 68.88; H, 6.26; N, 13.39. Found: C, 69.01; H, 6.10; N, 13.58.

*4.1.7.8. 3-Hydroxy-3-[2-(1-methyl-1H-benzo[d]imidazol-2-yl)-2-oxoethyl]-1-(morpholinomethyl)indolin-2-one (**12 h**).* It was obtained from the reaction of **4e** [97] and **11a** as pale yellow solid with mp 168–170 °C and yield 77% (1.61 g). IR: ν_{max}/cm^{-1} 3283, 1717, 1686, 1612. ^{1}H NMR (DMSO-d_6) δ (ppm): 2.61 (br d, 4H, morpholinyl 2 NCH_2), 3.57 (br s, 4H, morpholinyl 2 OCH_2), 3.81 (d, $J = 16.3$ Hz, 1H upfield H of CH_2CO), 3.83 (s, 3H, NCH_3), 4.38–4.44 (m, 3H, NCH_2N + downfield H of CH_2CO), 6.40 (s, 1H, OH), 6.95 (t, $J = 6.8$ Hz, 1H, arom. H), 7.14 (d, $J = 7.5$ Hz, 1H, arom. H), 7.26 (t, $J = 6.7$ Hz, 1H, arom. H), 7.36 (br s, 2H, arom. H), 7.42 (t, $J = 7.1$ Hz, 1H, arom. H), 7.62 (d, $J = 8.0$ Hz, 1H, arom. H), 7.84 (d, $J = 7.9$ Hz, 1H, arom. H). ^{13}C NMR (DMSO-d_6) δ (ppm): 31.8 (NCH_3), 46.9 (CH_2CO), 50.6 (morpholinyl NCH_2), 61.4 (NCH_2N), 66.1 (morpholinyl OCH_2), 72.9 (indolyl *C*-3) 109.8, 111.5, 121.2, 122.1, 123.4, 123.6, 125.7, 129.1, 130.4, 136.7, 140.8, 143.9, 145.5 (arom. *C*), 177.4 [indolyl *CO* (*C*-2)], 191.2 (ketonic *CO*). Anal. Calcd. for $C_{23}H_{24}N_4O_4$ (420.47): C, 65.70; H, 5.75; N, 13.33. Found: C, 65.51; H, 5.81; N, 13.47.

*4.1.8. Acidic dehydration of **12a-h** (general procedure)*

Hydrochloric acid (25 ml, 25%) was added dropwise (10 min.) to a magnetically stirred solution of **12a-h** (5 mmol) in absolute ethanol (12.5 ml) at room temperature (20–25 °C). The reaction mixture was kept stirring under the same conditions for 4 h and stored overnight at room temperature. The separated solid was collected, washed with

water and crystallized from a suitable solvent affording the corresponding **13a-f**.

*4.1.8.1. (E)-3-[2-(1-Methyl-1H-benzo[d]imidazol-2-yl)-2-oxoethylidene] indolin-2-one (**13a**).* It was obtained from acidic dehydration of **12a**, **12 g** or **12 h** as colorless microcrystals from *N*,*N*-dimethylformamide with mp 349–350 °C and yield 84, 73, 77% (1.27, 1.10, 1.16 g from reaction of **12a**, **12 g** and **12 h**, respectively). IR: ν_{max}/cm^{-1} 3124, 1694, 1585. ^{1}H NMR (CF_3CO_2D) δ (ppm): 4.26 (s, 3H, NCH_3), 7.57–7.91 (m, 6H, arom. H), 8.21 (d, $J = 8.4$ Hz, 1H, arom. H), 8.66 (s, 1H, olefinic H), 8.83 (d, $J = 8.5$ Hz, 1H, arom. H), 11.50 (s, 1H, NH). ^{13}C NMR (CF_3CO_2D) δ (ppm): 35.3 (NCH_3), 114.9, 116.8, 125.4, 128.4, 1629.0, 130.4, 131.2, 131.7, 132.4, 135.4, 136.0, 136.5, 141.1, 141.6, 146.0 (arom. *C* + olefinic C), 149.8 [indolyl *C*O (*C*-2)], 171.6 (ketonic *C*O). Anal. Calcd. for $C_{18}H_{13}N_3O_2$ (303.32): C, 71.28; H, 4.32; N, 13.85. Found: C, 71.49; H, 4.46; N, 14.01.

*4.1.8.2. (E)-3-[2-(1-Ethyl-1H-benzo[d]imidazol-2-yl)-2-oxoethylidene] indolin-2-one (**13b**).* It was obtained from acidic dehydration of **12b** as colorless microcrystals from *n*-butanol with mp 301–303 °C and yield 75% (1.19 g). IR: ν_{max}/cm^{-1} 3129, 1697, 1589. ^{1}H NMR (CF_3CO_2D) δ (ppm): 1.75 (t, $J = 7.2$ Hz, 3H, NCH_2CH_3), 4.99 (q, $J = 7.2$ Hz, 2H, NCH_2), 7.70–7.76 (m, 2H, arom. H), 7.84–7.85 (m, 2H, arom. H), 7.94 (t, $J = 7.7$ Hz, 1H, arom. H), 8.03 (t, $J = 7.6$ Hz, 1H, arom. H), 8.35 (d, $J = 8.5$ Hz, 1H, arom. H), 8.81 (s, 1H, olefinic H), 8.99 (d, $J = 8.7$ Hz, 1H, arom. H), 11.50 (s, 1H, NH). ^{13}C NMR (CF_3CO_2D) δ (ppm): 15.5 (CH_3), 45.0 (NCH_2), 114.7, 116.6, 124.7, 127.9, 128.4, 130.7, 131.17, 131.22, 132.4, 134.8, 135.0, 135.6, 142.0, 145.9 (arom. *C* + olefinic C), 150.5 [indolyl *C*O (*C*-2)], 171.9 (ketonic *C*O). Anal. Calcd. for $C_{19}H_{15}N_3O_2$ (317.35): C, 71.91; H, 4.76; N, 13.24. Found: C, 71.79; H, 4.68; N, 13.05.

*4.1.8.3. (E)-5-Chloro-3-[2-(1-methyl-1H-benzo[d]imidazol-2-yl)-2-oxoethylidene]indolin-2-one (**13c**).* It was obtained from acidic dehydration of **12c** as colorless microcrystals from *N*,*N*-dimethylformamide with mp 354–356 °C and yield 98% (1.65 g). IR: ν_{max}/cm^{-1} 3117, 1694, 1585. ^{1}H NMR (CF_3CO_2D) δ (ppm): 4.42 (s, 3H, NCH_3), 7.63–7.81 (m, 5H, arom. H), 8.17 (d, $J = 9.0$ Hz, 1H, arom. H), 8.77 (s, 1H, olefinic H), 8.91 (br s, 1H, arom. H), 11.50 (s, 1H, NH). ^{13}C NMR (CF_3CO_2D) δ (ppm): 35.3 (NCH_3), 114.7, 116.6, 125.8, 127.0, 128.8, 130.8, 131.4, 132.2, 133.7, 136.09, 136.14, 137.6, 142.4, 143.0, 147.1 (arom. *C* + olefinic C), 149.9 [indolyl *C*O (*C*-2)], 171.8 (ketonic *C*O). Anal. Calcd. for $C_{18}H_{12}ClN_3O_2$ (337.76): C, 64.01; H, 3.58; N, 12.44. Found: C, 63.85; H, 3.39; N, 12.30.

*4.1.8.4. (E)-5-Chloro-3-[2-(1-ethyl-1H-benzo[d]imidazol-2-yl)-2-oxoethylidene]indolin-2-one (**13d**).* It was obtained from acidic dehydration of **12d** as colorless microcrystals from *N*,*N*-dimethylformamide with mp 325–327 °C and yield 93% (1.63 g). IR: ν_{max}/cm^{-1} 3129, 1694, 1585. ^{1}H NMR (CF_3CO_2D) δ (ppm): 1.77 (t, $J = 7.2$ Hz, 3H, NCH_2CH_3), 5.04 (q, $J = 7.1$ Hz, 2H, NCH_2), 7.69–7.75 (m, 2H, arom. H), 7.83–7.91 (m, 3H, arom. H), 8.24 (d, $J = 9.1$ Hz, 1H, arom. H), 8.85 (s, 1H, olefinic H), 9.01 (d, $J = 1.8$ Hz, 1H, arom. H), 11.50 (s, 1H, NH). ^{13}C NMR (CF_3CO_2D) δ (ppm): 15.5 (CH_3), 45.0 (NCH_2), 114.6, 116.5, 125.4, 126.9, 128.6, 130.6, 131.1, 132.3, 133.8, 134.9, 135.9, 137.3, 142.2, 143.0, 146.4 (arom. *C* + olefinic C), 150.0 [indolyl *C*O (*C*-2)], 171.8 (ketonic *C*O). Anal. Calcd. for $C_{19}H_{14}ClN_3O_2$ (351.79): C, 64.87; H, 4.01; N, 11.94. Found: C, 64.76; H, 4.09; N, 11.77.

*4.1.8.5. (E)-5-Methoxy-3-[2-(1-methyl-1H-benzo[d]imidazol-2-yl)-2-oxoethylidene]indolin-2-one (**13e**).* It was obtained from acidic dehydration of **12e** as pale yellow microcrystals from *N*,*N*-dimethylformamide with mp 328–330 °C and yield 91% (1.52 g). IR: ν_{max}/cm^{-1} 3121, 1694, 1620. ^{1}H NMR (CF_3CO_2D) δ (ppm): 3.94 (s, 3H, OCH_3), 4.26 (s, 3H, NCH_3), 7.63–7.74 (m, 5H, arom. H), 8.19 (d, $J = 9.4$ Hz, 1H, arom. H), 8.37 (br s, 1H, arom. H), 8.78 (s, 1H, olefinic H), 11.50 (s, 1H, NH). ^{13}C NMR (CF_3CO_2D) δ (ppm): 35.1 (NCH_3), 57.9 (OCH_3), 106.0, 114.8, 116.7, 126.8, 130.3, 131.2, 131.4, 131.7, 132.2, 132.4, 135.8, 136.3, 138.9, 145.0, 145.2 (arom. *C* + olefinic C), 166.3 [indolyl *C*O (*C*-2)], 171.1 (ketonic *C*O). Anal. Calcd. for $C_{19}H_{15}N_3O_3$ (333.35): C, 68.46; H, 4.54; N, 12.61. Found: C, 68.61; H, 4.68; N, 12.53.

*4.1.8.6. (E)-3-[2-(1-Ethyl-1H-benzo[d]imidazol-2-yl)-2-oxoethylidene]-5-methoxyindolin-2-one (**13f**).* It was obtained from acidic dehydration of **12f** as pale yellow microcrystals from *N*,*N*-dimethylformamide with mp 317–319 °C and yield 95% (1.65 g). IR: ν_{max}/cm^{-1} 3121, 1694, 1620. ^{1}H NMR (CF_3CO_2D) δ (ppm): 1.63 (t, $J = 7.2$ Hz, 3H, NCH_2CH_3), 3.96 (s, 3H, OCH_3), 4.82 (q, $J = 7.1$ Hz, 2H, NCH_2), 7.61–7.66 (m, 3H, arom. H), 7.75 (t, $J = 5.9$ Hz, 2H, arom. H), 8.18 (d, $J = 9.4$ Hz, 1H, arom. H), 8.38 (d, $J = 2.4$ Hz, 1H, arom. H), 8.77 (s, 1H, olefinic H), 11.50 (s, 1H, NH). ^{13}C NMR (CF_3CO_2D) δ (ppm): 15.6 (CH_3), 45.1 (NCH_2), 57.8 (OCH_3), 105.9, 114.8, 116.8, 126.2, 130.3, 130.9, 131.4, 131.7, 132.6, 134.8, 137.4, 137.8, 145.3, 146.3 (arom. *C* + olefinic C), 165.9 [indolyl *C*O (*C*-2)], 171.6 (ketonic *C*O). Anal. Calcd. for $C_{20}H_{17}N_3O_3$ (347.37): C, 69.15; H, 4.93; N, 12.10. Found: C, 68.96; H, 4.75; N, 11.99.

4.2. X-ray studies

Mentioned in details in the supplementary file.

4.3. Biological studies

Mentioned in details in the supplementary file.

4.4. Docking studies

Mentioned in details in the supplementary file.

Declaration of Competing Interest

The authors declare that they have no known competing financial interests or personal relationships that could have appeared to influence the work reported in this paper.

Acknowledgments

This work was supported financially by National Research Centre, Egypt, project ID: 12060101.

Appendix A. Supplementary material

Supplementary data to this article can be found online at https://doi.org/10.1016/j.bioorg.2021.105131.

References

[1] A. Millemagg, R.J.K. Taylor, 3-Alkenyl-oxindoles: Natural products, pharmaceuticals, and recent Synthetic advances in tandem/telescoped approaches, Eur. J. Org. Chem. 4527–4547 (2010).
[2] https://www.drugs.com/history/sutent.html.
[3] https://www.cancer.gov/about-cancer/treatment/drugs/sunitinibmalate.
[4] E. Buchy, S. Valetti, S. Mura, J. Mougin, C. Troufflard, P. Couvreur, D. Desmaële, Synthesis and cytotoxic activity of self-assembling squalene conjugates of 3-[(pyrrol-2-yl)methylidene]-2,3-dihydro-1*H*-indol-2-one anticancer agents, Eur. J. Org. Chem. 202–212 (2015).
[5] https://www.who.int/news-room/fact-sheets/detail/cancer.
[6] https://www.who.int/health-topics/cancer#tab=tab_1.
[7] G. Chen, Q. Weng, L. Fu, Z. Wang, P. Yu, Z. Liu, X. Li, H. Zhang, G. Liang, Synthesis and biological evaluation of novel oxindole-based RTK inhibitors as anti-cancer agents, Bioorg. Med. Chem. 22 (2014) 6953–6960.
[8] R.-G. Fu, Y. Sun, W.-B. Sheng, D.-F. Liao, Designing multi-targeted agents: An emerging anticancer drug discovery paradigm, Eur. J. Med. Chem. 136 (2017) 195–211.
[9] T. Wang, X.-H. Liu, J. Guan, S. Ge, M.-B. Wu, J.-P. Lin, L.-R. Yang, Advancement of multi-target drug discoveries and promising applications in the field of Alzheimer's disease, Eur. J. Med. Chem. 169 (2019) 200–223.

[10] Y. Shan, C. Wang, L. Zhang, J. Wang, M. Wang, Y. Dong, Expanding the structural diversity of diarylureas as multi-target tyrosine kinase inhibitors, Bioorg. Med. Chem. 24 (2016) 750–758.
[11] S.S. Panda, A.S. Girgis, S.J. Thomas, J.E. Capito, R.F. George, A. Salman, M.A. El-Manawaty, A. Samir, Synthesis, pharmacological profile and 2D-QSAR studies of curcumin-amino acid conjugates as potential drug candidates, Eur. J. Med. Chem. 196 (2020), 112293.
[12] N.G. Fawzy, S.S. Panda, W. Fayad, E.M. Shalaby, A.M. Srour, A.S. Girgis, Synthesis, human topoisomerase IIα inhibitory properties and molecular modeling studies of anti-proliferative curcumin mimics, RSC Adv. 9 (2019) 33761–33774.
[13] N.G. Fawzy, S.S. Panda, W. Fayad, M.A. El-Manawaty, A.M. Srour, A.S. Girgis, Novel curcumin inspired antineoplastic 1-sulfonyl-4-piperidones: design, synthesis and molecular modeling studies, Anti-Cancer Agents Med. Chem. 19 (2019) 1069–1078.
[14] https://www.cancer.gov/about-cancer/treatment/drugs/belinostat.
[15] https://www.drugs.com/history/beleodaq.html.
[16] https://www.cancer.gov/about-cancer/treatment/drugs/dabrafenib.
[17] https://www.drugs.com/history/tafinlar.html.
[18] https://www.cancer.gov/about-cancer/treatment/drugs/pazopanibhydrochloride.
[19] https://www.drugs.com/history/votrient.html.
[20] https://www.cancer.gov/about-cancer/treatment/drugs/vemurafenib.
[21] https://www.drugs.com/history/zelboraf.html.
[22] https://www.cancer.gov/about-cancer/treatment/drugs/venetoclax.
[23] https://www.drugs.com/history/venclexta.html.
[24] N.S. Goud, S.M. Ghouse, J. Vishnu, D. Komal, V. Talla, R. Alvala, J. Pranay, J. Kumar, I.A. Qureshi, M. Alvala, Synthesis of 1-benzyl-1*H*-benzimidazoles as galectin-1 mediated anticancer agents, Bioorg. Chem. 89 (2019), 103016.
[25] J.E. Cheong, M. Zaffagni, I. Chung, Y. Xu, Y. Wang, F.E. Jernigan, B.R. Zetter, L. Sun, Synthesis and anticancer activity of novel water soluble benzimidazole carbamates, Eur. J. Med. Chem. 144 (2018) 372–385.
[26] L.-T. Wu, Z. Jiang, J.-J. Shen, H. Yi, Y.-C. Zhan, M.-Q. Sha, Z. Wang, S.-T. Xue, Z.-R. Li, Design, synthesis and biological evaluation of novel benzimidazole-2-substituted phenyl or pyridine propyl ketene derivatives as antitumour agents, Eur. J. Med. Chem. 114 (2016) 328–336.
[27] E. Łukowska-Chojnacka, P. Wińska, M. Wielechowska, M. Poprzeczko, M. Bretner, Synthesis of novel polybrominated benzimidazole derivatives- potential CK2 inhibitors with anticancer and proapoptotic activity, Bioorg. Med. Chem. 24 (2016) 735–741.
[28] V.K.A. Kalalbandi, J. Seetharamappa, 1-[(2*E*)-3-Phenylprop-2-enoyl]-1*H*-benzimidazoles as anticancer agents: synthesis, crystal structure analysis and binding studies of the most potent anticancer molecule with serum albumin, Med. Chem. Commun. 6 (2015) 1942–1953.
[29] Y.K. Yoon, M.A. Ali, A.C. Wei, T.S. Choon, H. Osman, K. Parang, A.N. Shirazi, Synthesis and evaluation of novel benzimidazole derivatives as sirtuin inhibitors with antitumor activities, Bioorg. Med. Chem. 22 (2014) 703–710.
[30] W. Wang, D. Kong, H. Cheng, L. Tan, Z. Zhang, X. Zhuang, H. Long, Y. Zhou, Y. Xu, X. Yang, K. Ding, New benzimidazole-2-urea derivates as tubulin inhibitors, Bioorg. Med. Chem. Lett. 24 (2014) 4250–4253.
[31] S. Dettmann, K. Szymanowitz, A. Wellner, A. Schiedel, C.E. Müller, R. Gust, 2-Phenyl-1-[4-(2-piperidine-1-yl-ethoxy)benzyl]-1*H*-benzimidazoles as ligands for the estrogen receptor: Synthesis and pharmacological evaluation, Bioorg. Med. Chem. 18 (2010) 4905–4916.
[32] R. Sharma, A. Bali, B.B. Chaudhari, Synthesis of methanesulphonamido-benzimidazole derivatives as gastro-sparing antiinflammatory agents with antioxidant effect, Bioorg. Med. Chem. Lett. 27 (2017) 3007–3013.
[33] K.Y. Yeong, C.W. Ang, M.A. Ali, H. Osman, S.C. Tan, Antituberculosis agents bearing the 1,2-disubstituted benzimidazole scaffold, Med. Chem. Res. 26 (2017) 770–778.
[34] B. Park, D. Awasthi, S.R. Chowdhury, E.H. Melief, K. Kumar, S.E. Knudson, R. A. Slayden, I. Ojima, Design, synthesis and evaluation of novel 2,5,6-trisubstituted benzimidazoles targeting FtsZ as antitubercular agents, Bioorg. Med. Chem. 22 (2014) 2602–2612.
[35] V.K.A. Kalalbandi, J. Seetharamappa, U. Katrahalli, K.G. Bhat, Synthesis, crystal studies, anti-tuberculosis and cytotoxic studies of 1-[(2*E*)-3-phenylprop-2-enoyl]-1*H*-benzimidazole derivatives, Eur. J. Med. Chem. 79 (2014) 194–202.
[36] A.M. Monforte, L. De Luca, M.R. Buemi, F.E. Agharbaoui, C. Pannecouque, S. Ferro, Structural optimization of N_1-aryl-benzimidazoles for the discovery of new non-nucleoside reverse transcriptase inhibitors active against wild-type and mutant HIV-1 strains, Bioorg. Med. Chem. 26 (2018) 661–674.
[37] T. Pan, X. He, B. Chen, H. Chen, G. Geng, H. Luo, H. Zhang, C. Bai, Development of benzimidazole derivatives to inhibit HIV-1 replication through protecting APOBEC3G protein, Eur. J. Med. Chem. 95 (2015) 500–513.
[38] A.-M. Monforte, S. Ferro, L. De Luca, G.L. Surdo, F. Morreale, C. Pannecouque, J. Balzarini, A. Chimirri, Design and synthesis of N_1-aryl-benzimidazoles 2-substituted as novel HIV-1 non-nucleoside reverse transcriptase inhibitors, Bioorg. Med. Chem. 22 (2014) 1459–1467.
[39] M. Özil, C. Parlak, N. Baltaş, A simple and efficient synthesis of benzimidazoles containing piperazine or morpholine skeleton at C-6 position as glucosidase inhibitors with antioxidant activity, Bioorg. Chem. 76 (2018) 468–477.
[40] N.K.N.A. Zawawi, M. Taha, N. Ahmat, N.H. Ismail, A. Wadood, F. Rahim, Synthesis, molecular docking studies of hybrid benzimidazole as α-glucosidase inhibitor, Bioorg. Chem. 70 (2017) 184–191.
[41] N.K.N.A. Zawawi, M. Taha, N. Ahmat, A. Wadood, N.H. Ismail, F. Rahim, S. S. Azam, N. Abdullah, Benzimidazole derivatives as new α-glucosidase inhibitors and in silico studies, Bioorg. Chem. 64 (2016) 29–36.
[42] A.S. Alpan, S. Parlar, L. Carlino, A.H. Tarikogullari, V. Alptüzün, H.S. Güneş, Synthesis, biological activity and molecular modeling studies on 1*H*-benzimidazole derivatives as acetylcholinesterase inhibitors, Bioorg. Med. Chem. 21 (2013) 4928–4937.
[43] E. Menteşe, F. Yılmaz, M. Emirik, S. Ülker, B. Kahveci, Synthesis, molecular docking and biological evaluation of some benzimidazole derivatives as potent pancreatic lipase inhibitors, Bioorg. Chem. 76 (2018) 478–486.
[44] A.A. Adegboye, K.M. Khan, U. Salar, S.A. Aboaba, S. Kanwal, I. Chigurupati, M. Fatima, A. Taha, J.I. Wadood, H. Mohammad, S. Perveen Khan, 2-Aryl benzimidazoles: Synthesis, In vitro α-amylase inhibitory activity, and molecular docking study, Eur. J. Med. Chem. 150 (2018) 248–260.
[45] V. Abbhi, L. Saini, S. Mishra, G. Sethi, A.P. Kumar, P. Piplani, Design and synthesis of benzimidazole-based Rho kinase inhibitors for the treatment of glaucoma, Bioorg. Med. Chem. 25 (2017) 6071–6085.
[46] https://www.drugs.com/history/treanda.html.
[47] https://www.cancer.gov/about-cancer/treatment/drugs/bendamustinehydrochloride.
[48] https://www.wcrf.org/dietandcancer/cancer-trends/pancreatic-cancer-statistics.
[49] https://www.cancer.gov/types/pancreatic.
[50] N. Vale, A. Correia-Branco, B. Patrício, D. Duarte, F. Martel, In vitro studies on the inhibition of colon cancer by amino acid derivatives of bromothiazole, Bioorg. Med. Chem. Lett. 27 (2017) 3507–3510.
[51] A.S. Girgis, S.S. Panda, I.S. Ahmed Farag, A.M. El-Shabiny, A.M. Moustafa, N.S. M. Ismail, G.G. Pillai, C.S. Panda, C.D. Hall, A.R. Katritzky, Synthesis, and QSAR analysis of anti-oncological active spiro-alkaloids, Org. Biomol. Chem. 13 (2015) 1741–1753.
[52] M. Liu, C.S. Scanlon, R. Banerjee, N. Russo, R.C. Inglehart, A.L. Willis, S.J. Weiss, N.J. D'Silva, The histone methyltransferase EZH2 mediates tumor progression on the chick chorioallantoic membrane assay, a novel model of head and neck squamous cell carcinoma, Transl. Oncol. 6 (2013) 273–281.
[53] C. Busch, J. Krochmann, U. Drews, The chick embryo as an experimental system for melanoma cell invasion, PLoS ONE 8 (2013), e53970.
[54] M. Schmiech, S.J. Lang, J. Ulrich, K. Werner, L.J. Rashan, T. Syrovets, T. Simmet, Comparative investigation of frankincense nutraceuticals: Correlation of boswellic and lupeolic acid contents with cytokine release inhibition and toxicity against triple-negative breast cancer cells, Nutrients 11 (2019) 2341.
[55] M. El Gaafary, S. Hafner, S.J. Lang, L. Jin, O.M. Sabry, C.V. Vogel, C.D. Vanderwal, T. Syrovets, T. Simmet, A novel polyhalogenated monoterpene induces cell cycle arrest and apoptosis in breast cancer cells, Mar. Drugs 17 (2019) 437.
[56] A.C. Estrada, T. Syrovets, K. Pitterle, O. Lunov, B. Büchele, J. Schimana-Pfeifer, T. Schmidt, S.A.F. Morad, T. Simmet, Tirucallic acids are novel pleckstrin homology domain-dependent Akt inhibitors inducing apoptosis in prostate cancer cells, Mol. Pharmacol. 77 (2010) 378–387.
[57] T. Syrovets, J.E. Gschwend, B. Büchele, Y. Laumonnier, W. Zugmaier, F. Genze, T. Simmet, Inhibition of IκB kinase activity by acetyl-boswellic acids promotes apoptosis in androgen-independent PC-3 prostate cancer cells *in Vitro* and *in Vivo*, J. Biol. Chem. 280 (2005) 6170–6180.
[58] WHO Director-General's Opening Remarks at the Media Briefing on COVID-19. https://www.who.int/dg/speeches/detail/who-director-general-s-opening-remarks-at-the-media-briefing-on-covid-19—11-march-2020.
[59] M. Wang, R. Cao, L. Zhang, X. Yang, J. Liu, M. Xu, Z. Shi, Z. Hu, W. Zhong, G. Xiao, Remdesivir and chloroquine effectively inhibit the recently emerged novel coronavirus (2019-nCoV) in vitro, Cell Res. 30 (2020) 269–271.
[60] M.S. Hosseini-Zare, R. Thilagavathi, C. Selvam, Targeting severe acute respiratory syndrome-coronavirus (SARS-CoV-1) with structurally diverse inhibitors: a comprehensive review, RSC Adv. 10 (2020) 28287–28299.
[61] https://covid19.who.int/ (accessed on May 17, 2021).
[62] G. Das, S. Ghosh, S. Garg, S. Ghosh, A. Jana, R. Samat, N. Mukherjee, R. Roya, S. Ghosh, An overview of key potential therapeutic strategies for combat in the COVID-19 battle, RSC Adv. 10 (2020) 28243–28266.
[63] P. Liu, H. Liu, Q. Sun, H. Liang, C. Li, X. Deng, Y. Liu, L. Lai, Potent inhibitors of SARS-CoV-2 3C-like protease derived from *N*-substituted isatin compounds, Eur. J. Med. Chem. 206 (2020), 112702.
[64] P. Gougis, C. Fenioux, C. Funck-Brentano, M. Veyri, J. Gligorov, C. Solas, J.-P. Spano, Anticancer drugs and COVID-19 antiviral treatments in patients with cancer: What can we safely use? Eur. J. Cancer 136 (2020) 1–3.
[65] M. Aldea, J.-M. Michot, F.-X. Danlos, A. Ribas, J.-C. Soria, Repurposing of anticancer drugs expands possibilities for antiviral and anti-inflammatory discovery in COVID-19, Cancer Discov. (in press, doi:10.1158/2159-8290.CD-21-0144).
[66] D. Díaz-Carballo, A.H. Acikelli, J. Klein, H. Jastrow, P. Dammann, T. Wyganowski, C. Guemues, S. Gustmann, W. Bardenheuer, S. Malak, N.S. Tefett, V. Khosrawipour, U. Giger-Pabst, A. Tannapfel, D. Strumberg, Therapeutic potential of antiviral drugs targeting chemorefractory colorectal adenocarcinoma cells overexpressing endogenous retroviral elements, J. Exp. Clin. Cancer Res. 34 (2015) 81.
[67] N.S.M. Ismail, R.F. George, R.A.T. Serya, F.N. Baselious, M. El-Manawaty, E. M. Shalaby, A.S. Girgis, Rational design, synthesis and 2D-QSAR studies of antiproliferative tropane-based compounds, RSC Adv. 6 (2016) 101911–101923.
[68] C. Marinaccio, D. Ribatti, A simple method of image analysis to estimate CAM vascularization by APERIO ImageScope software, Int. J. Dev. Biol. 59 (2015) 217–219.
[69] Y. Zhang, Y. Chen, D. Zhang, L. Wang, T. Lu, Y. Jiao, Discovery of novel potent VEGFR-2 inhibitors exerting significant antiproliferative activity against cancer cell lines, J. Med. Chem. 61 (2018) 140–157.
[70] A.-M. O'Farrell, J.M. Foran, W. Fiedler, H. Serve, R.L. Paquette, M.A. Cooper, H. A. Yuen, S.G. Louie, H. Kim, S. Nicholas, M.C. Heinrich, W.E. Berdel, C. Bello,

M. Jacobs, P. Scigalla, W.C. Manning, S. Kelsey, J.M. Cherrington, An innovative phase I clinical study demonstrates inhibition of FLT3 phosphorylation by SU11248 in acute myeloid leukemia patients, Clin. Cancer Res. 9 (2003) 5465–5476.
[71] J. Caballero, C. Muñoz, J.H. Alzate-Morales, S. Cunha, L. Gano, R. Bergmann, J. Steinbach, T. Kniess, Synthesis, *in silico*, *in vitro*, and *in vivo* investigation of 5-[^{11}C]methoxy-substituted sunitinib, a tyrosine kinase inhibitor of VEGFR-2, Eur. J. Med. Chem. 58 (2012) 272–280.
[72] T. Jiang, J. Zhuang, H. Duan, Y. Luo, Q. Zeng, K. Fan, H. Yan, D. Lu, Z. Ye, J. Hao, J. Feng, D. Yang, X. Yan, CD146 is a coreceptor for VEGFR-2 in tumor angiogenesis, Blood 120 (2012) 2330–2339.
[73] P. Carmeliet, R.K. Jain, Molecular mechanisms and clinical applications of angiogenesis, Nature 473 (2011) 298–307.
[74] C. Fontanella, E. Ongaro, S. Bolzonello, M. Guardascione, G. Fasola, G. Aprile, Clinical advances in the development of novel VEGFR2 inhibitors, Ann. Transl. Med. 2 (2014) 123–132.
[75] M. Shibuya, Vascular endothelial growth factor (VEGF) and its receptor (VEGFR) signaling in angiogenesis: A crucial target for anti- and pro-angiogenic therapies, Genes & cancer 2 (2011) 1097–1105.
[76] A.-K. Olsson, A. Dimberg, J. Kreuger, L. Claesson-Welsh, VEGF receptor signaling in control of vascular function, Nat. Rev. Mol. Cell Biol. 7 (2006) 359–371.
[77] S. Ravez, S. Arsenlis, A. Barczyk, A. Dupont, R. Frédérick, S. Hesse, G. Kirsch, P. Depreux, L. Goossens, Synthesis and biological evaluation of di-aryl urea derivatives as c-Kit inhibitors, Bioorg. Med. Chem. 23 (2015) 7340–7347.
[78] D.R. Minor, M. Kashani-Sabet, M. Garrido, S.J. O'Day, O. Hamid, B.C. Bastian, Sunitinib therapy for melanoma patients with KIT mutations, Clin. Canc. Res. : Off. J. Am. Assoc. Canc. Res. 18 (2012) 1457–1463.
[79] T. Abrams, A. Connor, C. Fanton, S.B. Cohen, T. Huber, K. Miller, E.E. Hong, X. Niu, J. Kline, M. Ison-Dugenny, S. Harris, D. Walker, K. Krauser, F. Galimi, Z. Wang, M. Ghoddusi, K. Mansfield, S.T. Lee-Hoeflich, J. Holash, N. Pryer, W. Kluwe, S. A. Ettenberg, W.R. Sellers, E. Lees, P. Kwon, J.A. Abraham, S.C. Schleyer, Preclinical antitumor activity of a novel anti–c-KIT antibody-drug conjugate against mutant and wild-type c-KIT-positive solid tumors, Clin. Canc. Res. : Off. J. Am. Assoc. Canc. Res. 24 (2018) 4297–4308.
[80] T.S. Kim, M.J. Cavnar, N.A. Cohen, E.C. Sorenson, J.B. Greer, A.M. Seifert, M. H. Crawley, B.L. Green, R. Popow, N. Pillarsetty, D.R. Veach, A.T. Ku, F. Rossi, P. Besmer, C.R. Antonescu, S. Zeng, R.P. DeMatteo, Increased KIT inhibition enhances therapeutic efficacy in gastrointestinal stromal tumor, Clin. Canc. Res. : Off. J. Am. Assoc. Canc. Res. 20 (2014) 2350–2362.
[81] S.J. Lee, T.-H. Jung, H. Kim, D. Jeong, G. Choi, W.-K. Park, J.Y. Kong, M.-H. Jin, H. Cho, Inhibition of c-Kit signaling by diosmetin isolated from *Chrysanthemum morifolium*, Arch. Pharm. Res. 37 (2014) 175–185.
[82] S.J. Modi, V.M. Kulkarni, Discovery of VEGFR-2 inhibitors exerting significant anticancer activity against CD44 and CD133 cancer stem cells (CSCs): Reversal of TGF-β induced epithelial-mesenchymal transition (EMT) in hepatocellular carcinoma, Eur. J. Med. Chem. 207 (2020), 112851.
[83] S. Ravez, A. Barczyk, P. Six, A. Cagnon, A. Garofalo, L. Goossens, P. Depreux, Inhibition of tumor cell growth and angiogenesis by 7-Aminoalkoxy-4-aryloxy-quinazoline ureas, a novel series of multi-tyrosine kinase inhibitors, Eur. J. Med. Chem. 79 (2014) 369–381.
[84] Propidium Iodide Flow Cytometrykit for cycle analysis, ab139418 (www.abcam.com).
[85] C. Bertoli, J.M. Skotheim, R.A.M. de Bruin, Control of cell cycle transcription during G1 and S phases, Nat. Rev. Mol. Cell Biol. 14 (2013) 518–528.
[86] Annexin V-FITC Apoptosis Detection Kit, Catalog#K101-25, www.biovision.com.
[87] M. Feoktistova, P. Geserick, M. Leverkus, Crystal violet assay for determining viability of cultured cells, Cold Spring Harb Protoc (2016), https://doi.org/10.1101/pdb.prot087379.
[88] A. Mostafa, A. Kandeil, Y.A.M.M. Elshaier, O. Kutkat, Y. Moatasim, A.A. Rashad, M. Shehata, M.R. Gomaa, N. Mahrous, S.H. Mahmoud, M. GabAllah, H. Abbas, A. El Taweel, A.E. Kayed, M.N. Kamel, M. El Sayes, D.B. Mahmoud, R. El-Shesheny, G. Kayali, M.A. Ali, FDA-approved drugs with potent in vitro antiviral activity against severe acute respiratory syndrome coronavirus 2, Pharmaceuticals 13 (2020) 443.
[89] R. Alnajjar, A. Mostafa, A. Kandeil, A.A. Al-Karmalawy, Molecular docking, molecular dynamics, and in vitro studies reveal the potential of angiotensin II receptor blockers to inhibit the COVID-19 main protease, Heliyon 6 (2020), https://doi.org/10.1016/j.heliyon.2020.e05641.
[90] https://www.rcsb.org/structure/4AGD.
[91] https://www.rcsb.org/structure/3G0E.
[92] M. McTigue, B.W. Murray, J.H. Chen, Y.-L. Deng, J. Solowiej, R.S. Kania, Molecular conformations, interactions, and properties associated with drug efficiency and clinical performance among VEGFR TK inhibitors, Proc. Natl. Acad. Sci. USA 109 (2012) 18281–18289.
[93] K.S. Gajiwala, J.C. Wu, J. Christensen, G.D. Deshmukh, W. Diehl, J.P. DiNitto, J. M. English, M.J. Greig, Y.-A. He, S.L. Jacques, E.A. Lunney, M. McTigue, D. Molina, T. Quenzer, P.A. Wells, X. Yu, Y. Zhang, A. Zou, M.R. Emmett, A.G. Marshall, H.-M. Zhang, G.D. Demetri, KIT kinase mutants show unique mechanisms of drug resistance to imatinib and sunitinib in gastrointestinal stromal tumor patients, Proc. Natl. Acad. Sci. USA 106 (2009) 1542–1547.
[94] Y. Tu, Y. Zhang, S. Xu, Z. Zhang, X. Xie, Cyanation of unactivated aryl chlorides and aryl mesylates catalyzed by palladium and hemilabile MOP-type ligands, Synlett (2014) 2938–2942.
[95] G.W.H. Cheeseman, 2-Acetylbenzimidazole, J. Chem. Soc. (1964) 4645–4646.
[96] Z.M. Nofal, A.M. Srour, W.I. El-Eraky, D.O. Saleh, A.S. Girgis, Rational design, synthesis and QSAR study of vasorelaxant active 3-pyridinecarbonitriles incorporating 1*H*-benzimidazol-2-yl function, Eur. J. Med. Chem. 63 (2013) 14–21.
[97] R.F. George, N.S.M. Ismail, J. Stawinski, A.S. Girgis, Design, synthesis and QSAR studies of dispiroindole derivatives as new antiproliferative agents, Eur. J. Med. Chem. 68 (2013) 339–351.